iScience

Article

A proteomic map of B cell activation and its shaping by mTORC1, MYC and iron

Highlights

- Comprehensive proteome resource for B cell activation
- Shared and distinct impacts of T cell-dependent and T cell-independent activation revealed
- Comparative analysis of mTORC1, MYC and iron modulation on B cell activation

Authors

Olivia J. James, Linda V. Sinclair, Nadejda Lefter, ..., Matteo Pecoraro, Greta Guarda, Andrew J.M. Howden

Correspondence

a.howden@dundee.ac.uk

In brief

Immunology; Molecular biology; Cell biology

James et al., 2026, iScience *29*, 118146
November 20, 2026 © 2026 The Authors. Published by Elsevier Inc.
https://doi.org/10.1016/j.isci.2026.118146

CellPress

iScience

CellPress
OPEN ACCESS

Article

A proteomic map of B cell activation and its shaping by mTORC1, MYC and iron

Olivia J. James,[1,5,6] Linda V. Sinclair,[1,6] Nadejda Lefter,[1] Anna A.C. Brock,[1] Fiamma Salerno,[2] Alejandro J. Brenes,[3] Hanif J. Khameneh,[4] Matteo Pecoraro,[4] Greta Guarda,[4] and Andrew J.M. Howden[1,7,*]

[1]Division of Cell Signalling and Immunology, Faculty of Life Sciences, University of Dundee, Dundee, UK
[2]Department of Immunology, Leiden University Medical Center, Leiden, the Netherlands
[3]Centre for Inflammation Research, Institute for Regeneration and Repair, University of Edinburgh, Edinburgh, UK
[4]Università della Svizzera Italiana (USI), Faculty of Biomedical Sciences, Institute for Research in Biomedicine, Bellinzona, Switzerland
[5]Present address: GSK, Gunnels Wood Road, Stevenage, UK
[6]These authors contributed equally
[7]Lead contact
*Correspondence: a.howden@dundee.ac.uk
https://doi.org/10.1016/j.isci.2026.118146

SUMMARY

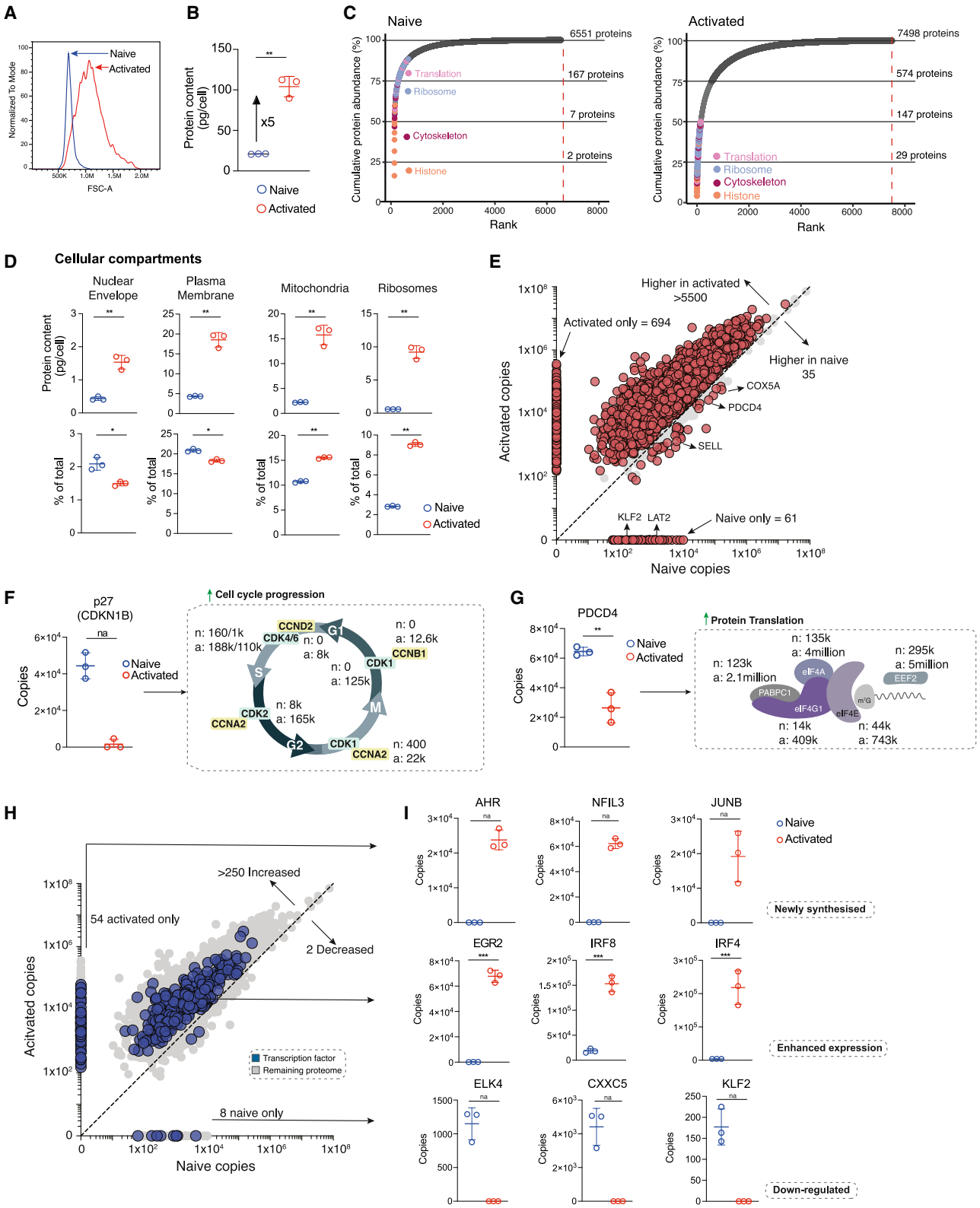
Using high-resolution quantitative mass spectrometry, we explored how immune activation and the metabolic regulator mTORC1 shape the B cell proteome. Activation through the B cell receptor, CD40, and the IL-4 receptor caused extensive remodeling of the protein landscape, including increased expression of metabolic machinery and nutrient transporters needed to support growth and biosynthesis. Comparing T cell-dependent and T cell-independent stimulation identified both shared and distinct pathways driving these changes. Inhibition of mTORC1 revealed an essential role in activation-induced B cell growth, amino acid transporter expression, and protein production. mTORC1 also regulated expression of the transcription factor MYC and the transferrin receptor CD71. Inhibiting MYC largely mirrored the effects of mTORC1 inhibition, while reduced iron availability impaired B cell growth and protein synthesis. These findings provide a comprehensive map of B cell proteome remodeling and reveal key roles for mTORC1, MYC and iron in supporting activation-induced growth and protein production.

INTRODUCTION

B lymphocytes (B cells) are a key component of the adaptive immune system, producing antibodies for targeting bacteria and viruses, secreting pro- and anti-inflammatory cytokines and presenting antigen to T cells.[1,2] B cell function is critical for maintaining health and, as such, B cell dysfunction is linked to a broad spectrum of diseases, including autoimmunity and immunodeficiency, diseases of the central nervous system, including multiple sclerosis, and B cell malignancies, including lymphomas and myelomas.[3–5] B cells sense and respond to their environment using a range of cell surface receptors. These receptors integrate antigen, co-stimulatory signals, cytokines, and environmental signals to mount an effective immune response.[2] Central to this environmental sensing is the B cell receptor (BCR), which, upon binding antigen, initiates signaling pathways that drive B cell activation, proliferation, and differentiation. However, B cell responses are also determined by other cell surface receptors, including CD40, which binds CD40 ligand expressed on the surface of T cells; pattern recognition Toll-like receptors, including TLR4, which is triggered by bacterial lipopolysaccharide; and cytokine receptors, including the interleukin-4 receptor (IL4R) and interleukin-21 receptor (IL21R). In many cases, these receptors act synergistically to direct B cell fate. For example, in germinal center B cells, both BCR and CD40 signals are required for robust induction of the transcription factor c-MYC (MYC), which in turn regulates cell cycle entry.[6] The cytokine environment also plays a key role in determining B cell activities. For example, IL4 directs B cell differentiation and immune responses, including antibody class switching[7] and the differentiation of memory B cell populations.[8,9] Several studies have attempted to dissect the shared and unique features of B cell stimuli along with their synergistic impacts, including the analysis of the transcriptional profile of different B cell stimuli, the dissection of downstream pathways regulated by BCR and co-stimulatory signals, and computational modeling to evaluate the impact of stimuli on B cell fate.[10–12] However, a systematic analysis of the impact of these stimuli on naive B cells and a deep analysis of how they regulate core cellular machinery and activation-induced proteome remodeling is missing.

Immune activation of B cells triggers naive cells to exit quiescence and undergo extensive transcriptional, translational, and metabolic reprogramming, driving proliferative expansion and B cell differentiation.[13–15] Effective B cell activation gives rise to populations of short- and long-lived antibody-producing

This is an open access article under the CC BY license (http://creativecommons.org/licenses/by/4.0/).



(legend on next page)

plasma cells as well as memory B cells.[2] Activated B cells need to ramp up metabolism and protein production appropriately to sustain these diverse fates.[14,16,17] A central metabolic regulator in mammalian cells is the nutrient-sensing serine/threonine protein kinase complex mTORC1, which integrates the nutritional status of the cell (nutrient and amino acid availability) and growth factor signals to regulate cellular protein synthesis and growth.[18] Various studies have outlined the importance of mTORC1 in B cell growth and differentiation, placing the nutrient-regulated kinase as a critical regulator of B cell function. mTORC1 is important in B cell class switching, somatic hypermutation, memory B cell formation, and the unfolded protein response.[19–23] However, the mechanistic details of how mTORC1 regulates B cell activation, metabolism, and protein synthesis are still to be fully mapped. While increasing evidence indicates that mTORC1 is essential for B cell functions, there are key gaps in our understanding of the downstream pathways impacted by mTORC1 in B cells and how these integrate with the fueling machinery required for B cell activation and differentiation. Given the cell-type and cell-context specific impacts of mTORC1, a detailed analysis of the role of mTORC1 in B cell activation is needed if we are to fully understand its importance during immune challenge.

Quantitative proteomics is a valuable tool to understand immune cell phenotypes and cellular responses to stimulation, stress, and the modulation of critical signaling pathways.[24–27] In this study, we use high-sensitivity quantitative mass spectrometry to map the activated B cell proteome. A comparative analysis of T cell-dependent versus T cell-independent stimulation on B cell proteome remodeling identifies differences in the scale of proteome remodeling along with selective impacts on protein expression. We also dissect the synergistic effect of B cell stimuli and provide new mechanistic insight into the additive impacts of B cell stimuli on metabolic machinery and proteome remodeling. To explore the metabolic regulation of B cell activation in more detail, we examined the role of mTORC1, MYC, and iron. mTORC1 inhibition dramatically impacts activation-induced proteome remodeling and impairs B cell protein production. mTORC1 activity is required for the sustained expression of the transcription factor MYC and for the upregulation of amino acid transporters that fuel B cell protein production. mTORC1 also regulates the expression of the transferrin receptor CD71, which is critical for iron uptake in cells. Inhibiting MYC phenocopies many of the effects of mTORC1 inhibition, including the reduced expression of CD71, while limiting iron availability during B cell activation impairs B cell growth and protein synthesis. We provide new insight into how B cells respond to BCR, TLR and co-stimulatory signals and modulate their core metabolic processes and machinery for fueling protein synthesis, shedding new light on the role of mTORC1, MYC and iron during B cell activation.

RESULTS

Activation-induced proteome remodeling in B cells

To assess the intrinsic changes driven by B cell activation, high-resolution quantitative mass spectrometry was used to characterize the proteomes of primary naive and immune-activated B cells, identifying and quantifying >7500 proteins. 24 h stimulation of B cells with anti-IgM, anti-CD40 and IL4 resulted in a considerable increase in B cell size as shown by flow cytometry (Figure 1A) and a 5-fold increase in total cellular protein mass (Figure 1B). Using the proteomic ruler,[28] we estimated the copy numbers per cell of all proteins identified in naive and activated B cells. Proteins were ranked according to their estimated copy number per cell and plotted against their cumulative contribution to total protein abundance, to evaluate which proteins

Figure 1. Activation-induced proteome remodeling in B cells

(A) Flow cytometry forward scatter (FSC) profiles of naive B cells (blue) and 24 h anti-IgM, anti-CD40 and IL4-activated B cells (red, referred to as "activated"). Data are representative of 3 biological replicates.

(B) Total protein content (pg/cell) of naive and 24 h activated B cells.

(C) Proteins ranked according to descending abundance and plotted against their cumulative abundance (shown as a percentage), for both naive and 24 h activated B cells. The number of proteins that make up each quartile of the proteome, summed with the quartile below, is shown in the designated section on each graph. Proteins making up the top-most 50% of activated B cells were annotated as either histones (orange), cytoskeletal (magenta), ribosomal (blue), or translational (pink) and were also mapped over the naive B cell plot.

(D) Top image shows the total protein mass (pg/cell) of proteins belonging to cellular compartments including nuclear envelope (GOCC:0005635), plasma membrane (GOCC:0005886), mitochondria (GOCC:0005739) and ribosomes (KEGG 03010) as per Gene Ontology/KEGG Orthology terms. Lower images show the % contribution to the total protein content for each term.

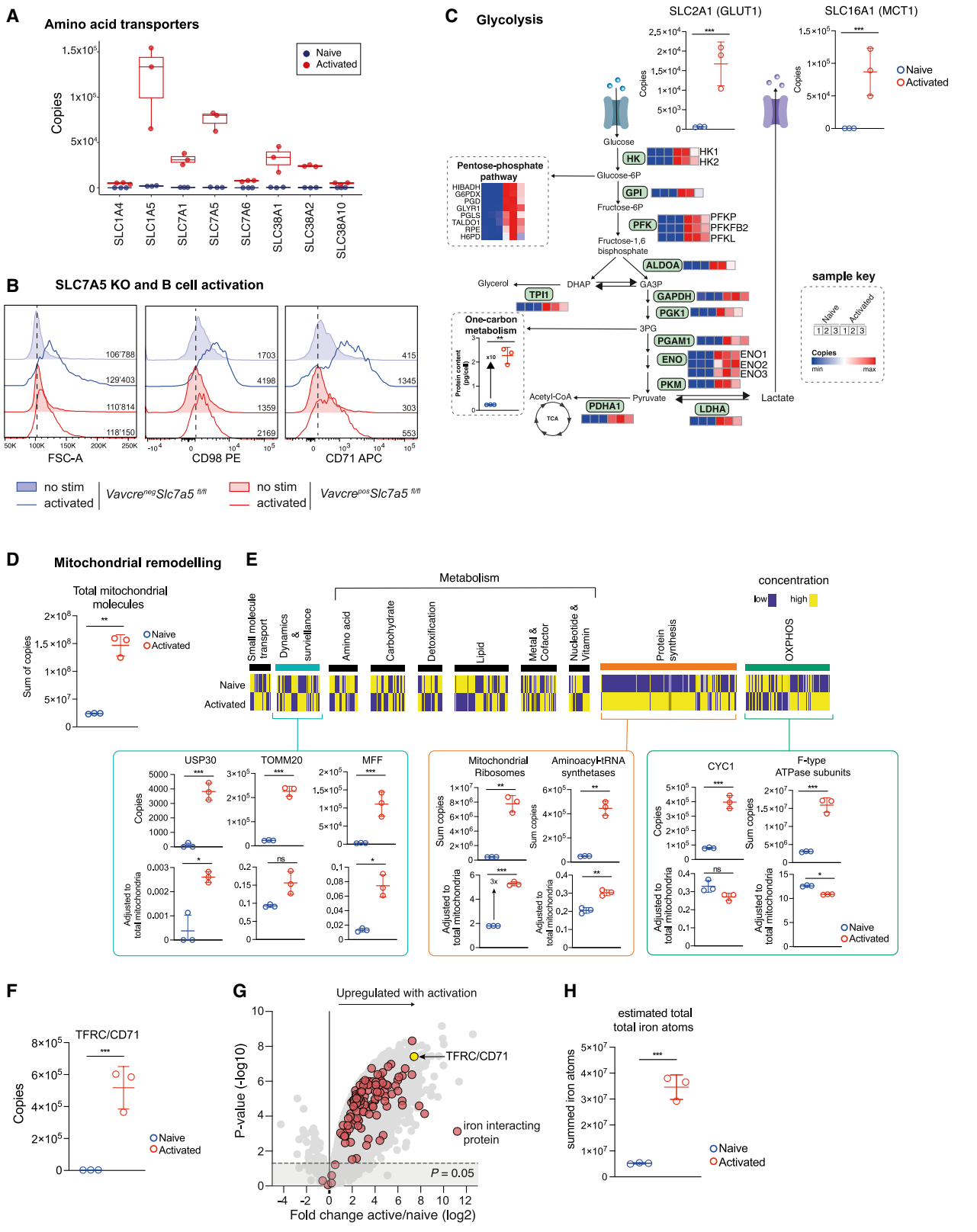
(E) Differential expression analysis between naive and activated B cells. Proteins were categorized as significantly changing between naive and 24 h activated B cells with a $p < 0.05$; fold change >1.5, or found in one population but not detected in the other population. Scatterplot shows the average protein copy number of each protein identified between naive and 24 h activated B cells. Proteins highlighted in red were significantly changing between naive and activated B cells. Proteins on the axes were found in one condition but not the other; numbers are provided on the plot for proteins found in 3/3 replicates of one condition.

(F) Expression data for the cyclin-dependent kinase inhibitor p27 (CDKN1B) and key regulators of the cell cycle.

(G) Expression data for components of the eIF4F translational complex, including the translational repressor PDCD4.

(H). Over 400 transcription factors and DNA-binding proteins were identified using the "Human transcription factor" list (ref: https://doi.org/10.1016/j.cell.2018.01.029) as a reference database. Scatterplot compares copy number expression profiles of the transcription factors (blue) between naive and 24 h activated B cells against the total proteome (gray). Proteins were categorized as significantly changing between naive and 24 h activated B cells with a $p < 0.05$; fold change >1.5 or found in one population but not detected in another population. Scatterplot shows the average protein copy number of each protein identified between naive and 24 h activated B cells.

(I) Histograms show protein copy numbers per cell for a selection of transcription factors such as those only expressed by activated B cells (newly synthesized), those with higher expression in activated as compared to naive B cells (enhanced expression), and those only expressed by naive B cells. For e, f, g, h and i, statistical significance was derived from two-tailed empirical Bayes moderated t-statistics performed in limma on the total dataset where $^{**}p < 0.01$ and $^{***}p < 0.001$. For b and d, statistical significance was derived from an unpaired two-tailed *t* test where $^{*}p < 0.05$ and $^{**}p < 0.01$. All data are from 3 biologically independent samples. All error bars are the mean with SD.



(legend on next page)

dominate the protein mass of naive and activated B cells (Figure 1C). In naive B cells, the 7 most abundant proteins, which contribute 50% of the total protein mass of the cell, are largely histones and cytoskeleton molecules, while in activated cells 147 proteins contribute 50% of the total protein mass and include ribosomal proteins and translational machinery, revealing that immune activation remodels the core proteome of B cells to drive protein synthesis (Figure 1C). To explore this further, we analyzed the contribution of different cellular compartments to the overall protein mass of the cell. Ribosomal proteins made up ~3% of the total protein mass of naive cells, which increased to 9% following activation, while mitochondrial proteins rose from 11% to 16% (Figure 1D). Some components such as the nuclear envelope and plasma membrane were present in higher copies following activation but when adjusted against the total cellular protein content, showed little change relative to the total proteome (Figure 1D).

To examine protein changes in more detail, differential expression analysis was performed and revealed that >5000 proteins were significantly increased in expression >1.5-fold and with a p value < 0.05 in activated B cells as compared to naive (Figure 1E). The full dataset along with fold changes and p values can be found in Data S1. Among those proteins increasing in abundance were activation receptors CD86, CD69, and CD44 (Data S1). 61 proteins were found exclusively in naive B cells and not in activated B cells, suggesting that they may be degraded upon B cell stimulation. These proteins included molecules controlling B cell quiescence such as the transcription factor KLF2[29–31] (Figure 1E). Only 35 proteins were significantly downregulated upon B cell activation. Among these downregulated proteins were negative regulators of key processes facilitating protein synthesis and proliferation such as the mRNA translational repressor PDCD4[32,33] and the cell cycle inhibitor p27 (CDKN1B) (Figures 1E–1G). The loss of p27 was accompanied by an increase in positive regulators of the cell cycle, such as cyclin-dependent kinases (CDK1-4), as well as A-type, B-type, and D-type cyclins (Figure 1F). Subunits of the EIF4F translational complex responsible for mRNA translation also showed an increase in abundance and a corresponding loss of PDCD4 (Figure 1G).

There was also considerable modulation of transcription factor expression upon B cell activation. Over 400 proteins with predicted transcription factor activity were identified within the dataset (Figure 1H and Data S1). Most of these transcription factors increased in abundance in response to immune activation, and some were only detected in activated cells, including NFIL3, AHR, and JUNB (Figures 1H and 1I). NFIL3 expression is regulated by IL4 and is critical for B cell class switching.[34] Other transcription factors were considerably upregulated upon activation, including IRF4, which increased from around 4,000 copies per cell in naïve B cells to over 200,000 copies per cell upon activation, and IRF8, which increased from approximately 20,000 copies to 150,000 copies. EGR2, which controls antigen receptor-induced proliferation in B cells,[35] increased from around 200 copies in naive cells to almost 70,000 copies upon activation. Some transcription factors increased by a much smaller scale, including PAX5 (Data S1), which increased less than 2-fold and which has previously been shown to be important during B cell development.[36,37] A small number of transcription factors were downregulated upon activation or were exclusively found in naive cells, including ELK4, CXXC5 and KLF2 (Figures 1H and 1I).

Immune activation drives nutrient transporter expression and metabolic and mitochondrial remodeling

24-h B cell activation was accompanied by a considerable increase in cell size and total protein content. This rapid increase in cell size is energetically demanding and would require increased uptake of nutrients to fuel anabolic processes. We next asked which nutrient and amino acid transporters were expressed in response to B cell activation. Several solute carrier (SLC) molecules were upregulated upon activation, including amino acid transporters SLC1A5, a glutamine transporter, and SLC7A5, which transports many essential amino acids including methionine, tryptophan, and leucine[38,39] (Figure 2A). Expression

Figure 2. B cell activation triggers metabolic and mitochondrial remodeling

(A) Boxplot shows the protein copy numbers per cell of a selection of amino acid transporters.

(B) The impact of deleting the amino acid transporter *Slc7a5* on B cell activation. Using flow cytometry, forward scatter and the expression of CD98/SLC3A2 and CD71 were analyzed in Vav cre$^+$ *Slc7a5*$^{fl/fl}$ (*Slc7a5* KO; red) and Vav cre$^-$ *Slc7a5*$^{fl/fl}$ (*Slc7a5* WT; blue) cells. Splenocytes were activated with anti-IgM and anti-CD40 (activated) or maintained in IL-7 (no stim).

(C) Schematic representation of the glycolytic pathway. Histograms show the protein copy number per cell for the glucose transporter GLUT1 (SLC2A1) and the lactate transporter MCT1 (SLC16A1). Copy number expression of key enzymes involved in glycolysis and the pentose phosphate shuttle is represented as a heatmap (lower expression is represented by blue and higher expression is represented by red; proteins not detected are shown as grey). Also shown is the total protein content (pg/cell) of proteins involved in one-carbon metabolism (GO:0006730).

(D) > 700 proteins were identified as belonging to the mitochondria as per the mouse MitoCarta 3.0 database.[40] The sum of all mitochondrial protein copy numbers per condition is presented.

(E) A ratio for the contribution of each mitochondrial protein to the total was calculated by dividing the copy number of each protein by the total mitochondrial molecules. This ratio was used to plot a heatmap showing relative expression from low (purple) to high (yellow). Heatmap was grouped based on the pathway annotations provided in MitoCarta 3.0. Histograms showing the protein copy numbers per cell and the associated ratio of the total for proteins in particular pathways are shown.

(F) Estimated copy numbers per cell for CD71(TFRC) in naive and activated B cells.

(G) The expression profile of proteins annotated as iron-interacting (red circles) in naive versus activated B cells.

(H) The estimated total iron atom requirement for those iron-interacting proteins identified within naive and activated B cells. For copy number comparisons of individual proteins statistical significance was derived from two-tailed empirical Bayes moderated t-statistics performed in limma on the total dataset where ***$p < 0.001$. For all other comparisons statistical significance was derived from an unpaired two-tailed t test where *$p < 0.05$, **$p < 0.01$, and ***$p < 0.001$. All data are from 3 biologically independent samples except B, which is representative of 2 biological replicates. All error bars are mean with SD.

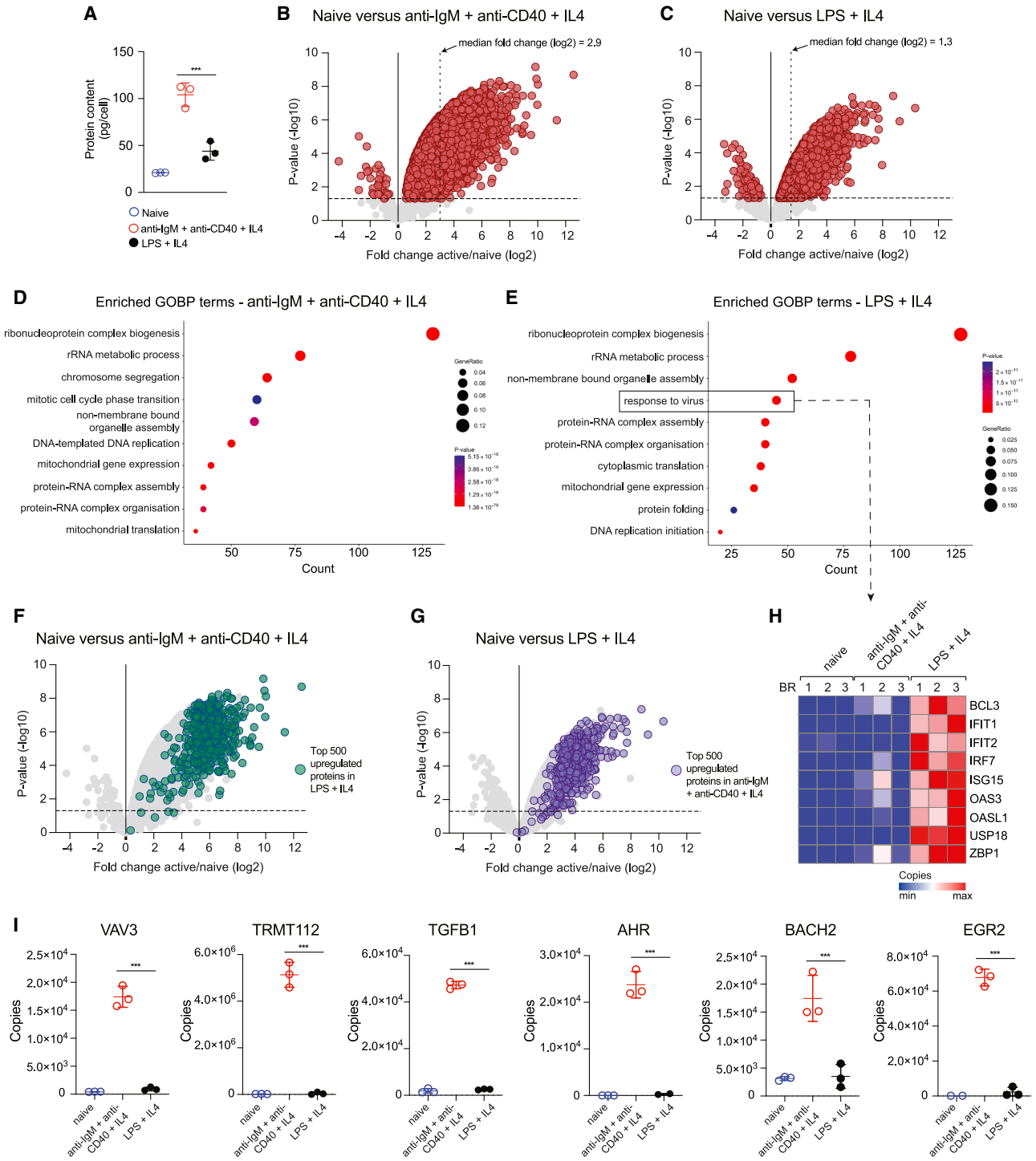


Figure 3. Shared and unique features of T cell-dependent versus T cell-independent B cell activation

(A) Total protein content (pg/cell) of naive B cells and B cells activated for 24 h with either anti-IgM + anti-CD40 + IL4 or LPS + IL4.

(B and C) Volcano plot shows the differential expression profile of proteins as a consequence of either (b) anti-IgM + anti-CD40 + IL4 versus naive or (c) LPS + IL4 versus naive. Data are presented as the log2 fold change of the copy number ratio (activated vs. naive B cells) against the significance value (-log10 *p* value). The median fold change is shown for each dataset as a dashed vertical line.

(D and E) GO enrichment analysis of proteins significantly upregulated in response to stimulation plus proteins only identified in activated B cells and absent in naive B cells. (D) Enriched GO terms in response to anti-IgM + anti-CD40 + IL4 or (E) LPS + IL4. Data shown are the top 10 most enriched GO pathways.

(legend continued on next page)

of these transporters was extremely low in naive B cells (Figure 2A). SLC7A5 is critical for antigen-driven T cell responses, T cell differentiation, and effector function.[41,42] To explore the importance of SLC7A5 in B cell activation, we used splenocytes from VavCre x *Slc7a5*$^{fl/fl}$ mice.[41] In these mice, VavCre drives deletion of *Slc7a5* in early hematopoietic development. Splenocytes from VavCre x *Slc7a5*$^{fl/fl}$ mice were activated using anti-IgM and anti-CD40. The *Slc7a5* KO B cells were considerably smaller than Cre-negative controls after activation (Figure 2B). *Slc7a5* KO B cells also showed reduced expression of CD98/SLC3A2, the heavy chain chaperone which forms a heterodimer with many amino acid transporters, including SLC7A5 and SLC7A6.[43] Additionally, *Slc7a5* KO B cells had impaired expression of the transferrin receptor CD71 in response to immune activation. CD71 is essential for iron uptake, which fuels multiple metabolic processes in B cells[44–46] (Figure 2B). Together, these data highlight the important role of a single amino acid transporter in fueling the increase in size and the upregulation of key proteins that fuel B cell immune activation.

We next wanted to understand in greater detail the metabolic shift in B cells that occurs upon activation.[16] Using estimates of protein copy per cell, we mapped glycolytic enzymes and enzymes that drive the pentose-phosphate pathway and one-carbon metabolism. Previous studies have questioned the importance of glycolysis in B cell activation, suggesting instead that activated B cells switch on oxidative phosphorylation and the tricarboxylic acid cycle (TCA cycle) but not glycolysis.[14] The proteomic data show that expression of the glycolytic machinery, including rate-limiting glucose and lactate transporters[47] as well as glycolytic enzymes, is considerably upregulated upon B cell activation (Figure 2C). Indeed, the glucose and lactate transporters SLC2A1 and SLC16A1 were virtually undetectable in naive cells but were found in tens of thousands of copies upon B cell activation (Figure 2C and Data S1). The cellular mass of enzymes involved in one-carbon metabolism increased 10-fold in response to B cell activation, suggesting changes in metabolic enzymes that are beyond just scaling with increased cell size (Figure 2C).

Activation-induced mitochondrial re-modelling has been well documented in B cells.[14,16,48,49] Using Mitocarta,[40] predicted mitochondrial proteins were annotated within our dataset, revealing that total mitochondrial molecules increased approximately 6-fold upon B cell activation (Figure 2D). To explore changes in mitochondrial processes that were independent of activation-induced mitochondrial scaling, we adjusted protein copy numbers by the total mitochondrial protein molecules to determine their relative contribution. This analysis revealed mitochondrial proteins and processes that did not just follow the scaled increase in mitochondrial mass (Figure 2E). For example, mitochondrial ribosomes increased 3-fold when adjusted against total mitochondrial molecules, suggesting increased dedication toward mitochondrial protein synthesis in the activating cell. In contrast, molecules involved in oxidative phosphorylation showed a diverse expression pattern, with some, including cytochrome *c*1 and F-type ATPase subunits, remaining at similar concentrations in naive and activated B cells, suggesting a scaled increase in abundance (Figure 2E).

Having noted significant increases in amino acid, glucose, and lactate transporter expression upon B cell activation (Figures 2A and 2C) we also found considerable upregulation of the transferrin receptor CD71 (TFRC) from around 3000 copies per cell in naive B cells to approximately 0.5 million copies upon activation (Figure 2F). Using annotations of iron-regulated proteins,[50] we examined the expression profile of iron-interacting proteins in naive and activated B cells. We detected 151 iron-regulated proteins in our proteomics data. These included proteins involved in Fe-S cluster synthesis, histone modification (Jmjd family proteins, Kdm family proteins), DNA synthesis (Pol family proteins), and OXPHOS (Figure 2G and Data S1). To gain a clearer understanding of the cellular requirements for iron, we estimated the total iron content of the naive and activated B cells. We assumed that all iron-interacting sites were fully occupied and used known values of iron atoms per protein (where possible). Where exact values were not known, we used a deliberate underestimation of 1 iron atom for heme or iron ion interaction, and 2 iron atoms for Fe-S cluster interactions.[50] Using the protein copy numbers from our data, these calculations showed that the iron demand, or requirement, in naive B cells is approximately 5 million iron atoms per cell. The demand for iron is increased 7-fold to 35 million iron atoms per cell in activated B cells (Figure 2H). These increased requirements for iron, to drive DNA synthesis, histone modifications and mitochondrial functions, are matched by the increased expression of CD71 (TFRC).

The selective effects of T cell-dependent versus T cell-independent activation

Next, we compared the impact of T cell-dependent versus T cell-independent activation. Naive B cells were activated with the TLR4 ligand, lipopolysaccharide (LPS), along with IL4, and the proteome was mapped after 24 h. The total protein content approximately doubled in response to LPS and IL4 stimulation compared with a 5-fold increase in response to anti-IgM, anti-CD40 and IL4 (Figure 3A). The difference in the scale of proteome remodeling was also reflected in differential expression analysis, with anti-IgM, anti-CD40 and IL4 triggering a median increase in protein abundance greater than 7.4-fold (log2 fold change = 2.9) (Figure 3B), while LPS and IL4 stimulation triggered a median fold change of 2.4 (log2 fold change = 1.3) (Figure 3C). A key question was whether the same proteins and processes were regulated by T cell-dependent versus independent activation. Enrichment analysis of upregulated proteins revealed that almost identical

(F and G) Comparative analysis of the expression profile of proteins between two stimulation conditions. (F) Top 500 upregulated proteins in response to LPS + IL4 were examined for their expression in response to anti-IgM + anti-CD40 + IL4. (G) The top 500 upregulated proteins in response to anti-IgM + anti-CD40 + IL4 were examined for their expression in response to LPS + IL4.

(H) The expression profile of proteins annotated as "response to virus" across naive and activated populations.

(I) The expression profile of a selection of proteins across naive and activated populations. For b, c, f, g and i, differential expression analysis and statistical significance were derived from two-tailed empirical Bayes moderated t-statistics performed in limma on the total dataset. For a, statistical significance was derived from an unpaired two-tailed *t* test where ***$p < 0.001$. All data are from 3 biologically independent samples. All error bars are mean with SD.

biological processes were significantly enriched regardless of the stimulation, with ribosomal and mitochondrial proteins along with DNA replication machinery being consistently increased in abundance (Figures 3D and 3E). Analysis of the top 500 proteins upregulated in response to either anti-IgM, anti-CD40 and IL4 or LPS and IL4 also revealed that almost all had the same pattern of expression in each stimulation condition (Figures 3F and 3G). However, important exceptions were identified. Notably, LPS and IL4 triggered the expression of interferon-regulated proteins, including IFIT1, IFIT2, ISG15, and OAS3 (Figure 3H). Anti-IgM, anti-CD40 and IL4 selectively upregulated a small number of proteins, including VAV3, which couples B cell receptor triggering to phosphoinositide 3-kinase signaling and calcium flux,[51] tRNA Methyltransferase Activator Subunit 11-2 (TRMT112), which is a key promoter of methyltransferase activity and Transforming Growth Factor β 1 (TGFB1), which has pleiotropic effects across immune cells including the regulation B cell activation, proliferation and differentiation. Interestingly, transcription factors that have important roles in regulating B cell fate were also specifically upregulated in response to anti-IgM, anti-CD40 and IL4 but not LPS and IL4. These include aryl hydrocarbon receptor (AHR) and BACH2, which regulate B cell class switching and B cell differentiation,[52,53] and EGR2 (Figure 3I). Together, these results highlight that the scale of proteome remodeling is drastically different upon T cell-dependent versus T cell-independent activation, and key determinants of B cell fate and B cell differentiation are selectively regulated.

The synergistic impact of B cell stimuli

Stimulating B cells with anti-IgM, anti-CD40 and IL4 caused substantial proteome remodeling. To dissect the synergistic effects of these stimuli, B cells were stimulated with anti-IgM, anti-CD40 and IL4 individually and in combinations, and their proteomes analyzed by single-shot mass spectrometry. Over 7000 proteins were identified across the experiment. As expected, triggering the B cell receptor with anti-IgM caused a down-regulation of the signaling subunits of the B cell receptor, CD79a and CD79b (Figures S1A and S1B), and an upregulation of the nuclear receptor NR4A3, which has previously been shown to be upregulated upon BCR triggering (Figure S1C). NFIL3 expression was induced only in conditions in which IL4 was present (Figure S1D). Together, these results provided confidence in the ability to identify selective effects of stimulation using this dataset. Next, we explored the impact of individual and combined stimuli on total protein abundance and the expression profile of proteins driving key cellular processes. B cell stimuli had additive effects on cellular protein abundance, with the addition of IL4 triggering a boost in protein synthesis (Figure 4A). IL4 promotes B cell survival, differentiation, and isotype class switching, and previous studies have revealed that IL4 induces MYC expression[54] and drives cholesterol metabolism in B cells.[55] Stimulating B cells with IL4 alone caused a modest increase in cell size, MYC expression and protein synthesis (Figures S1E–1G). However, IL4 in combination with anti-CD40 or anti-IgM induced a significant increase in the abundance of glycolytic enzymes, glucose and lactate transporters, and ribosomal proteins (Figures 4B and 4C). Maximal expression of these molecules was induced in B cells triggered through the BCR, CD40, and in the presence of IL4. Individually, each of these stimuli triggered a downregulation of the cell cycle inhibitor CDKN1B (P27) (Figure 4D). IL4 or anti-CD40 alone had little impact on cell cycle machinery but together triggered a modest increase in cyclins A2, B1, and B2 and CDK2, 4, 6, and 7. Anti-IgM in combination with IL4 or anti-CD40 was clearly the major driver of the expression of the cell cycle machinery (Figure 4D).

The transcription factor MYC is a central regulator of cellular protein synthesis and growth. As mentioned above, MYC expression was modestly induced by IL4 but its detection was challenging by mass spectrometry, particularly in cells stimulated with either IL4, anti-CD40, or anti-IgM alone. This is likely due to the rapid turnover of MYC within the cell and to these stimuli triggering small increases in MYC expression that are below the sensitivity of our mass spectrometry approach. However, combinations of stimuli resulted in increased expression of MYC and its binding partner MAX (Figures 4E and 4F). B cell receptor and CD40 triggering were required for maximal expression of MYC. Intriguingly, previous findings have revealed that MYC is induced by either BCR or CD40 signals in naive B cells but both signals are required for robust MYC induction in germinal center B cells.[6] A primary function of MYC in lymphocytes is the regulation of amino acid transporter expression.[56] Known MYC-regulated transporters, TFRC (CD71) and the methionine transporter SLC7A5, were maximally expressed in response to BCR and co-stimulatory signals (Figures 4G and 4H).

mTORC1 activity drives protein biosynthesis and the machinery for fueling B cells

Together, the B cell activation data reveal the complex interplay between B cell stimuli in driving protein synthesis and the remodeling of the core cellular machinery. Given the central role that mTORC1 plays in regulating diverse cellular responses, including lymphocyte growth and differentiation,[19,22,57–60] we next wanted to explore how mTORC1 regulates the protein biosynthetic capacity of activating B cells and the impact of blocking mTORC1 activity on B cell proteome remodeling. To selectively block mTORC1 during B cell activation, cells were treated with rapamycin for the first 24 h of activation, a time point that precedes activation-induced B cell division.[61,62] mTORC1 activity was monitored through the phosphorylation of ribosomal protein S6, a downstream target of active mTORC1 signaling. Blocking mTORC1 activity with rapamycin during B cell activation reduced S6 phosphorylation to levels similar to those observed in naive B cells (Figure 5A). Rapamycin-treated cells were significantly smaller in size and had approximately half the total cellular protein mass when compared to control activated cells (Figures 5B and 5C). Further, B cells activated with rapamycin exhibited a considerable reduction in rates of protein synthesis compared to control activated cells, as measured by the incorporation of an analog of puromycin into elongating protein chains in the ribosome (Figure 5D). We sought to understand how the inhibition of mTORC1 was driving the reduction in rates of protein synthesis and consequent decrease in protein mass. Proteomic analysis of cells treated with rapamycin revealed that >4700 proteins had reduced abundance when mTORC1 activity was blocked, while only 28 proteins were found at significantly increased levels (Figure 5E). GO term enrichment analysis revealed that mTORC1 inhibition had a profound effect on DNA

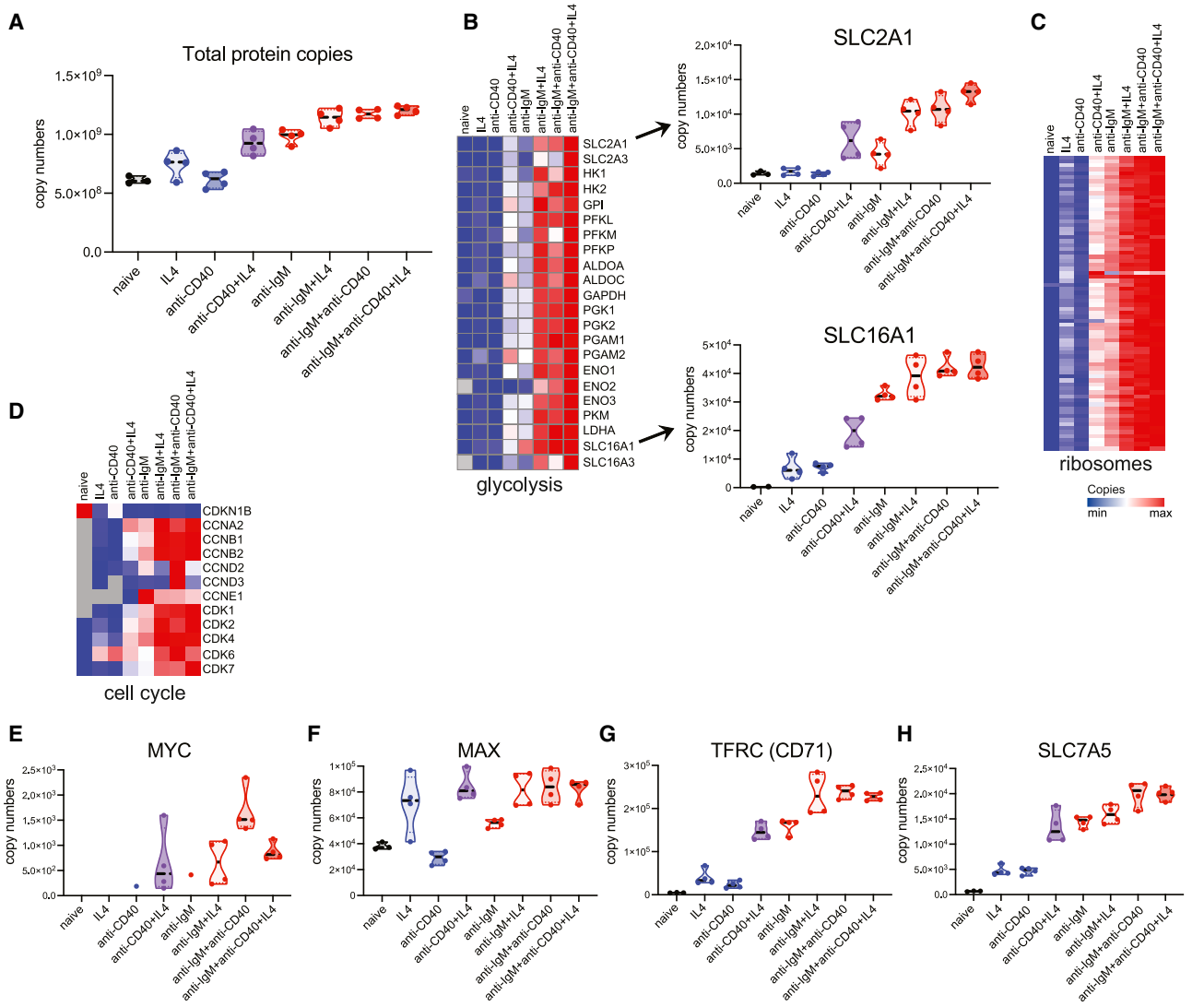


Figure 4. The synergistic impact of B cell stimuli

(A) Total protein copies per cell for naive B cells and B cells activated individually and with combinations of IL4, anti-IgM, and anti-CD40.

(B) Expression profile of proteins belonging to the glycolytic pathway, including glucose and lactate transporters.

(C) The impact of combinations of B cell stimuli on the expression of ribosomal proteins and (D) cell cycle machinery. The expression profile of MYC (E), MAX (F), TFRC (G), and SLC7A5 (H) in response to B cell stimuli. All data are from at least 3 biologically independent samples.

replication machinery and mitochondrial translation (Figure 5F). A closer examination revealed that ribosomal protein mass and mitochondrial protein mass were both significantly reduced in response to blocking mTORC1 (Figure 5G). Transcription factors were among some of the most rapamycin-sensitive proteins in B cells. IRF4, a critical regulator of B cell reprogramming during early activation,[63] was found at significantly lower levels in rapamycin-treated cells (Figure 5H). IRF8 expression was also significantly impaired when mTORC1 activity was blocked. IRF8 has previously been shown to be important during B cell development and B cell germinal center responses,[64–66] although the role of IRF8 during B cell activation remains unclear. Our proteomic data also revealed high expression of AHR exclusively in activated B cells, which was found at significantly reduced levels, along with the aryl hydrocarbon receptor nuclear translocator (ARNT), by rapamycin treatment (Figure 5I). AHR deletion has been shown to impact B cell proliferation.[67] Interestingly, several cyclin-dependent kinases were found at significantly reduced levels in response to mTORC1 inhibition, notably CDK1, which was found at over 120,000 copies per cell in activated B cells but only 5,000 copies in B cells activated with rapamycin (Data S1). Together, these data suggest that blocking mTORC1 with rapamycin significantly impacts activation-induced proteome remodeling, reducing the abundance of key proteins involved in ribosomal and mitochondrial mass, transcriptional regulation, proliferation, and cell cycle progression.

mTORC1 inhibition also resulted in reduced expression of multiple solute carrier proteins (Figure 5J), including the glucose

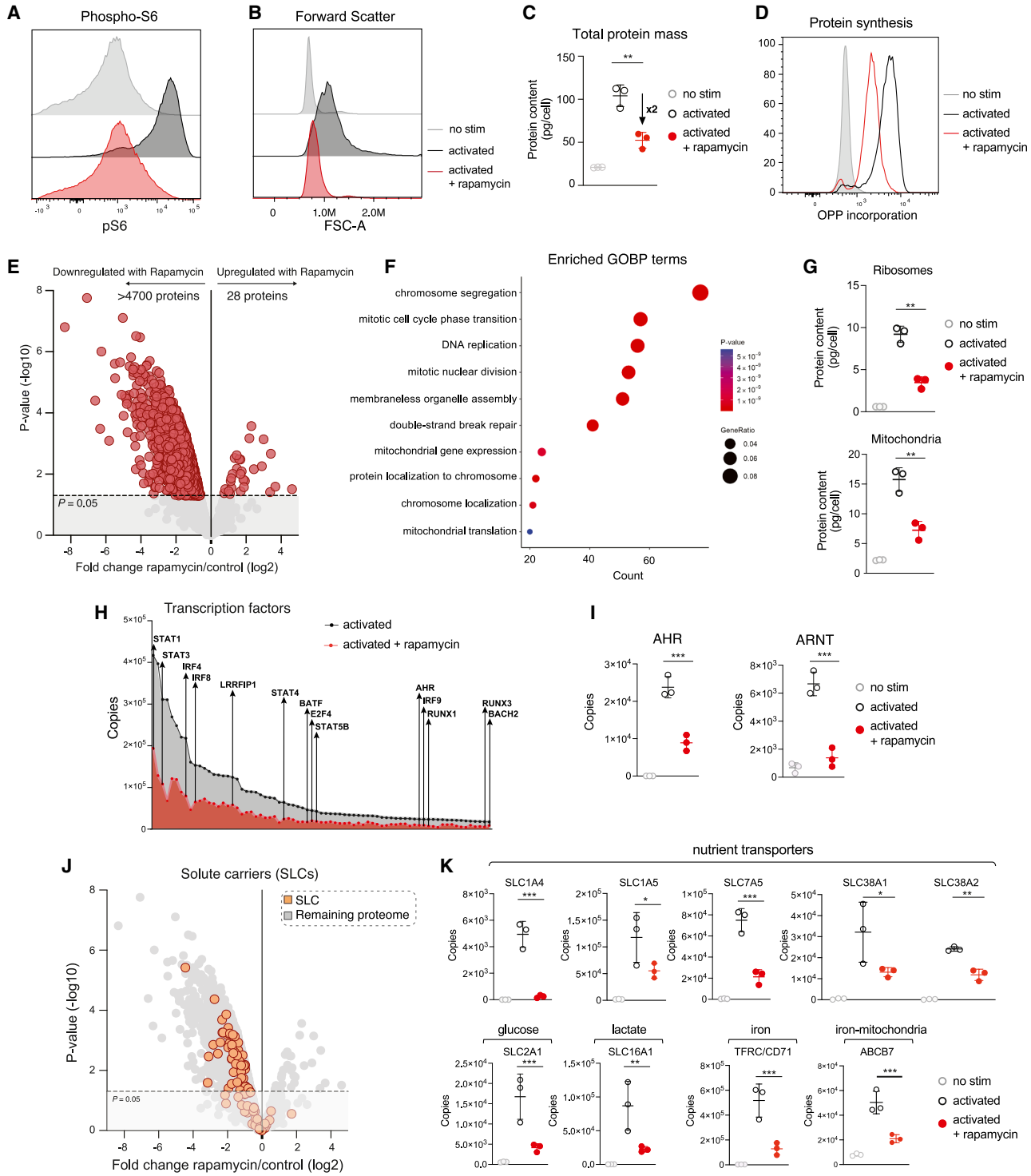


Figure 5. The mTORC1-regulated proteome

(A) Phosphorylation of S6 in non-stimulated (gray), activated (black), and activated + rapamycin (red) cells, as determined by flow cytometry.

(B) Flow cytometry forward scatter (FSC) profile of non-stimulated (gray), activated (black), and activated + rapamycin (red) cells.

(C) Total protein content (pg/cell) of naive and 24 h activated B cells ± rapamycin.

(D) Protein synthesis determined by O-propargyl-puromycin (OPP) incorporation into elongating protein chains and flow cytometry.

(E) Volcano plot shows the differential expression profile of proteins as a consequence of rapamycin treatment. Data are presented as the log2 fold change of the copy number ratio (rapamycin-treated vs. -untreated activated B cells) against the significance value (-log10 *p* value). Proteins were considered significantly

(legend continued on next page)

transporter SLC2A1, the lactate transporter SLC16A,1 and the System L amino acid transporter SLC7A5 (Figure 5K). Expression of the transferrin receptor CD71 and the mitochondrial iron transporter ABCB7 were also significantly reduced in abundance in response to mTORC1 inhibition (Figure 5K). To explore the impact of mTORC1 inhibition on amino acid transport further, we interrogated the System L amino acid transport capacity of B cells using a sensitive, flow cytometry-based assay.[68] Uptake of the fluorescent SLC7A5 substrate kynurenine was impaired in B cells activated in the presence of rapamycin, orthogonally validating our proteomics data showing reduced levels of SLC7A5 abundance (Figures 6A–6C). Flow cytometry analysis also revealed reduced abundance of CD98/SLC3A2 (Figures 6D and 6E) and the transferrin receptor CD71 (Figures 6F and 6G). We next assessed the expression of iron-interacting proteins in response to mTORC1 inhibition (Figure 6H) and found that many were considerably reduced in abundance, including dioxygenase enzymes ALKBH1-8, a selection of cytochromes, NDUF molecules that are critical for oxidative phosphorylation, along with components of the DNA replication fork complex (Figure 6H). Taken together, these data suggest that mTORC1 plays a crucial role in regulating the expression of multiple nutrient transporters in B cells, including transporters for glucose, lactate, amino acids, and iron, and regulating the expression of iron-interacting molecules.

mTORC1 regulates MYC expression in B cells

We questioned whether mTORC1-driven effects on nutrient and amino acid transport expression in B cells could in part be explained by an impact on MYC abundance. MYC is a master regulator of cellular metabolism and growth in T cells.[56] We monitored MYC expression in response to mTORC1 inhibition using an MYC-GFP reporter mouse.[69] We found that MYC was upregulated upon B cell activation but MYC expression was significantly reduced in rapamycin-treated cells at 4 h and 24 h (Figures 6I and 6J), suggesting that mTORC1 activity is required for maximal MYC expression during B cell activation. Having revealed that mTORC1 activity impacts MYC expression in activating B cells, we next sought to understand the consequence of directly blocking MYC activity on B cells. To block MYC at the point of activation, B cells were treated with a small molecule inhibitor of MYC, MYCi361, which inhibits the formation of MYC:MAX heterodimers and blocks the ability of MYC to bind DNA.[70] Mass spectrometry was used to evaluate the impact of MYC inhibition on the B cell protein landscape for the initial 24 h of activation (before activation-induced cell division), while flow cytometry of key surface markers was used for validation. B cells activated in the presence of MYCi361 were reduced in size compared to control cells, according to their forward scatter profile (Figure 7A), and total protein copies per cell were also reduced in response to MYC inhibition (Figure 7B). Over 2500 proteins showed reduced abundance when MYC activity was blocked (Figure 7C). Included in those proteins that were reduced in abundance were ribosomal proteins (Figure 7D). In activated B cells, ribosomal proteins totaled over 1.5×10^8 copies per cell, while in MYC inhibitor-treated cells this reduced to approximately 0.75×10^8 copies (Figure 7D). Components of the DNA replication fork machinery were also considerably reduced in expression upon MYC inhibition, in some cases more than 5-fold (Table 1). The impact of MYC inhibition on DNA replication proteins was strikingly similar when compared with rapamycin-treated cells (Table 1), highlighting the overlap between mTORC1- and MYC-regulated proteins in B cells. Enrichment analysis of those proteins downregulated in response to MYC inhibition showed striking overlap in biological processes regulated by MYC and mTORC1, with DNA replication and mitochondrial translation being consistently impacted (Figure S2). Analysis of the top 1000 proteins downregulated in response to either rapamycin or MYCi361 revealed an overlap of 30% of these proteins. However, closer examination revealed that almost all of the 1000 most downregulated proteins had the same pattern of expression in response to rapamycin or MYCi361 (Figure S2). To support the MYC inhibitor experiments, we explored the impact of *Myc* deletion on activation-induced proteome remodeling in B cells. The homing receptor CD62L was not impacted by MYCi361 or *Myc* deletion, while the activation marker CD69 was slightly elevated in response to MYCi361 or *Myc* deletion (Figures 7E–7J), in agreement with observations in activating MYC null T cells.[56] The transferrin receptor CD71 (TFRC), whose expression is dependent on MYC expression in CD8 T cells[71] and B cells,[72] showed reduced abundance in response to MYCi361 and *Myc* deletion (Figures 7K–7M). Additionally, expression of iron-interacting proteins was among those reduced upon MYC inhibition (Figure 7N). Interestingly, we noted that the transporters SLC7A5 and SLC2A1, which were both downregulated upon mTORC1 inhibition, were not impacted by MYC inhibition or deletion (Figures 7O–7R), indicating expression of these transporters in activated B cells is mTORC1 dependent but MYC independent.

differentially expressed if the fold change value > 1.5-fold in either an up- or down-regulated direction and if the p value < 0.05 (significance cutoff represented as a dashed line).

(F) GO enrichment analysis of proteins significantly downregulated plus proteins only identified in activated B cells and absent in rapamycin-treated B cells. Data shown are the top 10 most enriched GO BP pathways.

(G) Total protein content (pg/cell) of proteins belonging to mitochondria (GOCC:0005739) and ribosomes (KEGG 03010).

(H) Average copy number expression of a subset of transcription factors presented as a line plot between activated B cells ± rapamycin. Key transcription factors controlling B cell identity and differentiation are shown.

(I) Protein copy numbers for the Aryl Hydrocarbon receptor (AHR) and the Aryl hydrocarbon nuclear translocator (ARNT) in activated B cells ± rapamycin.

(J) Expression profile of solute carrier (SLC) proteins (orange) in response to rapamycin treatment. Log2 fold-change (rapamycin-treated vs. -untreated activated B cells) is plotted against the significance value (-log10 p value). p value < 0.05 is represented as a dashed line.

(K) Protein copy number per cell for a selection of key nutrient transporters for each condition: naive, 24 h activated, and rapamycin-treated B cells. For e, i, j and k, differential expression analysis and statistical significance was derived from two-tailed empirical Bayes moderated t-statistics performed in limma on the total dataset where $^*p < 0.05$, $^{**}p < 0.01$, and $^{***}p < 0.001$. For c and g, statistical significance was derived from an unpaired two-tailed t test where $^{**}p < 0.01$. All data are from 3 biologically independent samples. All error bars are the mean with SD. Data presented in d are representative of 3 biological replicates.

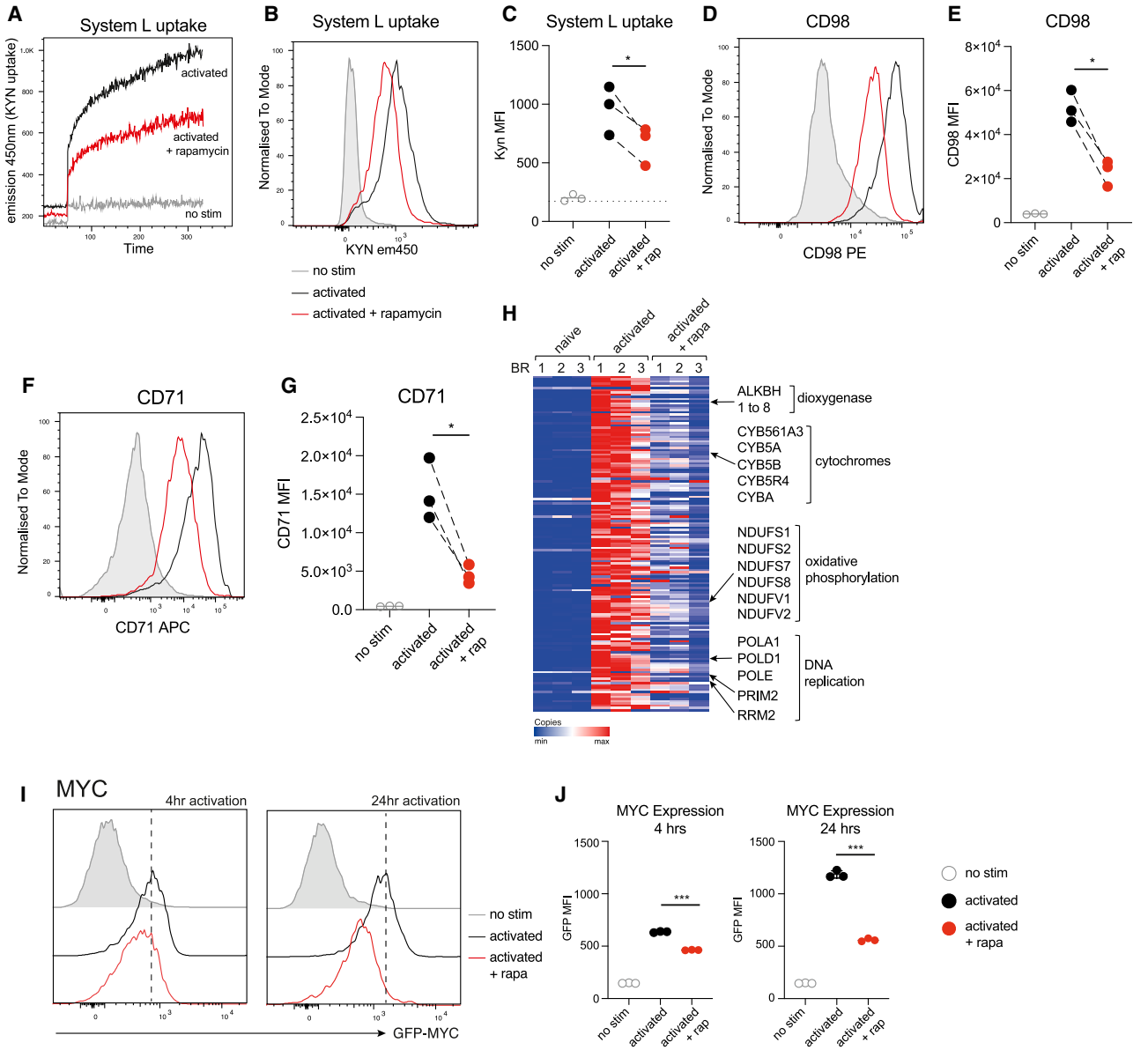


Figure 6. mTORC1 activity regulates amino acid uptake, iron-interacting proteins, and MYC expression

(A) Live flow cytometric monitoring of system L-dependent uptake in activated B cells ± rapamycin. B cells were activated for 24 hbefore the addition of the system L substrate kynurenine (KYN), and fluorescence emission (450 nm) was monitored over time. Unstimulated cells were included as a control.

(B and C) KYN uptake for 4 min and then fixed and analyzed by flow cytometry.

(D and E) The expression of CD98/SLC3A2 in non-stimulated and activated B cells ± rapamycin.

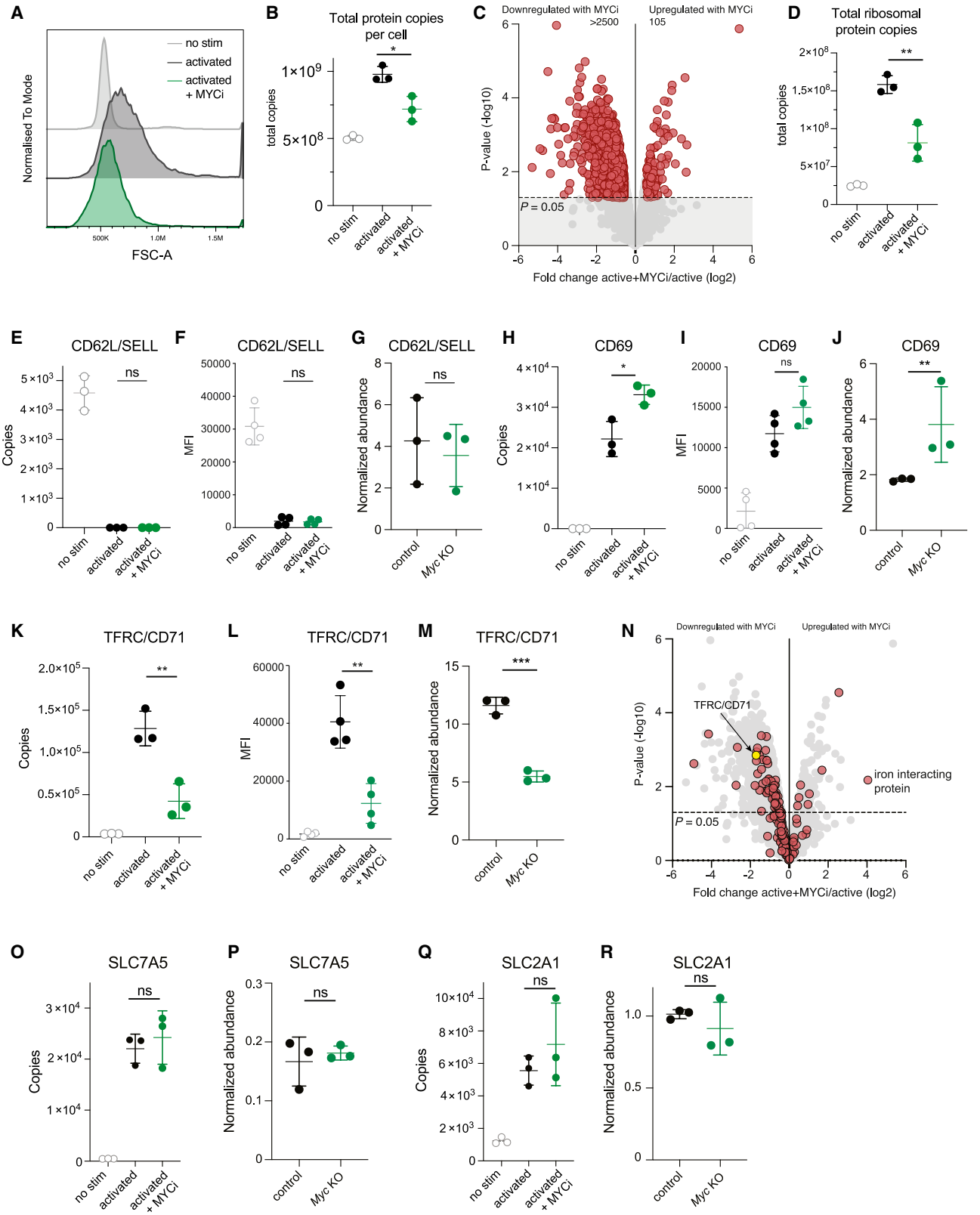
(F and G) The expression of CD71 in non-stimulated and activated B cells ± rapamycin.

(H) The expression profile of iron-interacting proteins in naive, activated, and activated + rapamycin B cells. A selection of iron-interacting protein categories are labeled on the heatmap.

(I and J) The impact of rapamycin treatment on MYC expression in activating B cells. B cells from GFP-tagged MYC mice were activated ± rapamycin, and MYC-GFP expression was monitored at 4 h and 24 h by flow cytometry. Statistical significance was derived from an unpaired two-tailed *t* test where $*p < 0.05$ and $***p < 0.001$. For all experiments, 3 biologically independent samples were analyzed.

Iron availability is essential for B cell growth and protein synthesis

Receptor-mediated endocytosis through the transferrin receptor CD71 is the primary method by which lymphocytes take up iron from their extracellular environment. Mutations in CD71 are linked with impaired lymphocyte function and immunodeficiency.[44] Having found that CD71 expression is regulated by MYC and mTORC1 activity and SLC7A5 expression, we next tested whether iron availability regulates activation-induced B cell growth and protein synthesis. Using the iron chelator



(legend on next page)

deferiprone (3-Hydroxy-1,2-dimethyl-4(1H)-pyridone) B cells were activated for 24 h in iron-depleting conditions and monitored by flow cytometry to assess cell size, activation, and protein synthesis. Iron chelation impaired the increase in cell size seen upon B cell activation, with increasing concentrations of deferiprone correlating with decreased cell size (Figures 8A–8C). However, B cells were still able to upregulate the activation marker CD69 in iron-limiting conditions (Figures 8D and 8E). Protein synthesis was significantly increased in activated B cells when compared with IL4-maintained cells but dropped with increasing concentration of the iron chelator (Figures 8F and 8G). Higher concentrations of deferiprone (100 μM and 300 μM) brought levels of protein synthesis down to levels seen in IL4-maintained cells. Together, these data show that iron availability is a critical regulator of activation-induced cell growth in B cells.

DISCUSSION

In this work, we have mapped the protein landscape of naive B cells and their response to activation through the B cell receptor, CD40, and the IL4 receptor. Our data reveal the scale of proteome remodeling triggered by B cell activation and the dramatic reconfiguration of cellular compartments, including mitochondria and ribosomes. This study aimed to identify the metabolic regulators of B cell activation and protein synthesis. One important biological insight was the identification of the repertoire of amino acid transporters that are expressed upon B cell activation. Deleting one of these transporters, *Slc7a5,* which transports methionine, tryptophan, and leucine, was catastrophic for B cell activation, further highlighting the critical role of this transporter in B cell responses. SLC7A5 has previously been shown to be important during B cell development, with *Slc7a5* knockdown mice showing reduced B1 B cell numbers.[73] SLC7A5 inhibition impacts B cell differentiation and antibody secretion and negatively impacts mTORC1 activity,[74] while deletion of *Slc3a2*, which forms a heterodimer with transporters including SLC7A5, suppresses B cell proliferation and plasma cell formation.[75] In a complementary study, Cheung et al. reveal the importance of SLC7A5 during LPS-mediated B cell activation, with *Slc7a5* KO B cells showing impaired activation and proliferation.[76] Together, our studies support previous findings showing the fundamental role of a single amino acid transporter in B cell activities.

We also explored the impact of different stimuli on B cell proteome remodeling. The scale of protein changes induced by LPS and IL-4 versus anti-IgM, anti-CD40, and IL-4 was markedly different. However, the cellular processes and pathways impacted by these two stimulation conditions were largely conserved. Notable exceptions included transcription factors driving B cell fate. An examination of the synergistic impacts of B cell stimuli revealed that glycolytic enzymes, ribosomal proteins, and cell cycle machinery were maximally expressed in response to co-stimulation. Interestingly, the expression of nutrient and amino acid transporters was minimally increased in response to anti-CD40 or IL4 but considerably increased in combination. IL4 is a known driver of protein synthesis in B cells. Our data suggest that this is in part due to the synergistic impact of IL4 inducing the expression of the nutrient and amino acid transporters required for fueling B cells, along with the machinery for protein synthesis and glycolysis.

To understand the metabolic regulation of B cells, we examined the impact of blocking mTORC1 activity during B cell activation. While mTORC1 is firmly established as a key regulator of metabolism and protein synthesis,[77,78] the mechanisms by which it does this in different cell types and at stages of cellular differentiation are yet to be fully mapped. In B cells, mTORC1 activity regulates the expression of the machinery for the unfolded protein response prior to B cell differentiation into plasma cells[23] and is an important regulator of plasma cell differentiation and humoral immunity.[79,80] In the current study, we wanted to explore the impact of mTORC1 inhibition during B cell activation. Inhibiting mTORC1 had a considerable impact on protein production during B cell activation, and cells activated in the presence of rapamycin had a reduction in total protein mass of approximately 50% compared to control activated cells. This was also reflected in a significant reduction in ribosomal protein mass in rapamycin-treated cells. We found that SLC7A5 expression was regulated by mTORC1, with rapamycin treated cells showing reduced abundance of SLC7A5 and reduced SLC7A5-mediated amino acid uptake. The impact of mTORC1 inhibition on amino acid transporters was generally greater in B cells than has been observed previously in T cells.[41,57] mTORC1 also regulates the expression of transcription factors that direct B cell activation and differentiation, including IRF's, AHR, and MYC. Our findings align with a previous study showing mTORC1-dependent regulation of MYC expression in developing B cells.[81] In T cells, the transcription factor MYC is

Figure 7. Blocking MYC activity impairs ribosomal protein mass and iron-interacting proteins

(A) Flow cytometry forward scatter (FSC) profile of non-stimulated (gray), activated (black), and activated + MYCi361 (green) cells.

(B) Total protein molecules per cell for naive and 24 h activated B cells ± MYCi361.

(C) Volcano plot showing the differential expression profile of proteins as a consequence of MYCi361 treatment. Data are presented as the log2 fold change of the copy number ratio (MYCi361-treated vs. -untreated activated B cells) against the significance value (-log10 *p* value). Proteins were considered significantly differentially expressed (highlighted in red) if the fold change value > 1.5-fold in either up- or down-regulated direction and if the *p* value < 0.05 (significance cutoff represented as a dashed line).

(D) Total ribosomal protein molecules per cell for naive and 24 h activated B cells ± MYCi361. The impact of MYCi361 or *Myc* deletion on CD62L (L-selectin), CD69, and CD71 (TFRC) measured by mass spectrometry (E, G, H, J, K, and M) and flow cytometry (F, I, and L). (N) Volcano plot showing the expression profile of iron-interacting proteins in response to blocking MYC activity.

(O–R) The impact of MYCi361 or *Myc* deletion on the abundance of SLC7A5 and SLC2A1. For b, d, f, I, and l statistical significance was derived from an unpaired two-tailed *t* test where $*p < 0.05$ and $**p < 0.01$. For all other experiments differential expression analysis and statistical significance was derived from two-tailed empirical Bayes moderated t-statistics performed in limma on the total dataset where $*p < 0.05$ and $**p < 0.01$. For all experiments, at least 3 biologically independent samples were analyzed. All error bars are mean with SD.

Table 1. The impact of mTORC1 inhibition and MYC inhibition on components of the DNA replication complex

Protein	Fold change activ + rapa/activ	*p* value	Fold change activ + MYCi/activ	*p* value
LIG1	0.26	<0.01	0.22	<0.01
MCM4	0.25	<0.001	0.23	<0.001
MCM5	0.3	<0.001	0.24	<0.001
MCM6	0.39	<0.01	0.24	<0.001
MCM7	0.27	<0.001	0.23	<0.001
PCNA	0.33	<0.001	0.39	<0.01
POLA1	0.17	<0.01	0.16	<0.001
POLD1	0.43	<0.01	0.57	<0.05
POLE	0.1	<0.001	0.09	<0.01
RFC3	0.33	<0.001	0.55	<0.05

The fold change and *p* value for a selection of key proteins are provided for activated B cells ± rapamycin and ± MYCi361. Statistical significance was determined using a two-tailed empirical Bayes moderated *t* test performed in limma on the total dataset.

required for the expression of SLC7A5, along with a selection of other nutrient transporters including CD71.[56] Inhibiting MYC activity in B cells phenocopied many of the mTORC1 inhibition effects, including a considerable impact on the cell's DNA replication machinery, ribosomal protein content, and the abundance of CD71. *Myc* deletion has previously been shown to impact activation-induced B cell growth and proliferation,[82] and our data suggest this in part may be driven by impacting CD71 expression and the machinery for proliferation and protein synthesis. However, we also revealed unique differences between mTORC1 and MYC inhibition in B cells, with MYC inhibition having little impact on the abundance of SLC7A5 and the glucose transporter SLC2A1. *Slc7a5* KO B cells fail to blast and fail to induce CD71 expression in response to BCR engagement. The observation that SLC7A5 expression is MYC-dependent in T cells but independent in B cells in response to antigen receptor activation suggests cell-specific regulation of this key amino acid transporter in lymphocytes. Interestingly, while mTORC1 and

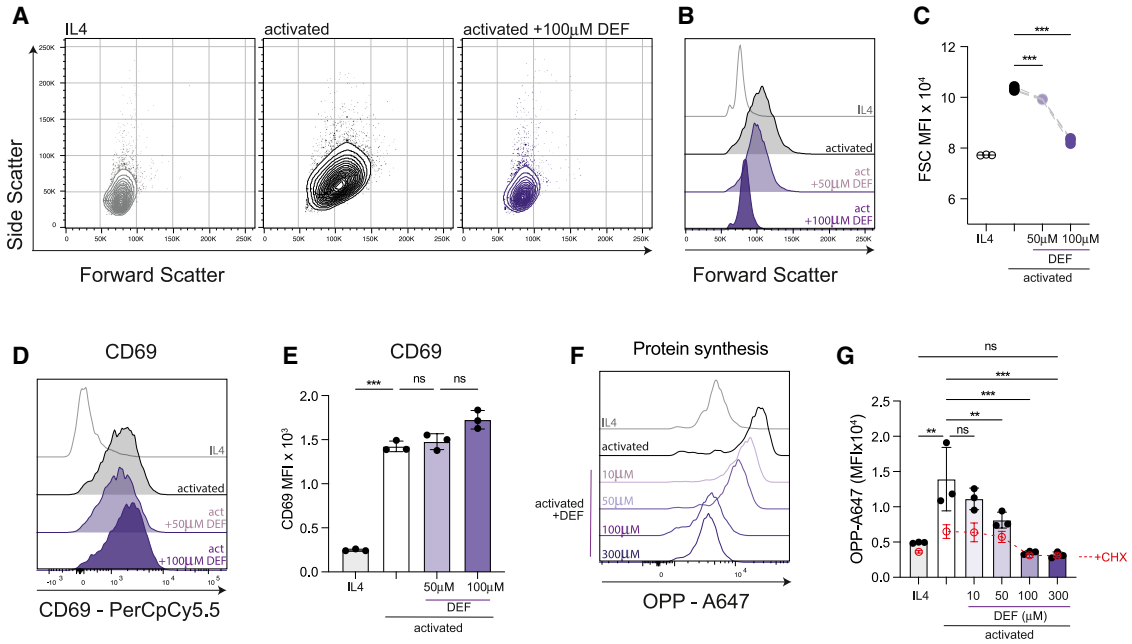


Figure 8. Iron availability is critical for activation-induced B cell growth and protein synthesis

(A) Flow cytometry forward and side scatter profile of B cells after 24 h either maintained in IL4 (1 ng/ml) or activated with anti-IgM, anti-CD40, and IL4 (10 ng/ml) +/− the iron chelator deferiprone.

(B and C) Forward scatter profile of B cells activated for 24 h as described above.

(D and E) CD69 expression in B cells after 24 h either maintained in IL4 (1 ng/ml) or activated with anti-IgM, anti-CD40, and IL4 (10 ng/ml) +/− deferiprone.

(F and G) The impact of deferiprone on B cell protein synthesis. B cells were activated for 24 h and protein synthesis was measured by OPP incorporation and labeling with Alexa 647-azide using a copper-catalyzed click-chemistry reaction. Cycloheximide (CHX) was included as an inhibitor of cytosolic protein synthesis. For all experiments 3 biologically independent samples were analyzed. All error bars are the mean with SD. Data in a, b, d, and f are representative of 3 biological replicates. Statistical significance was derived from one way ANOVA where $*p < 0.05$, $**p < 0.01$, and $***p < 0.001$.

MYC are considered master regulators of cellular metabolism, their inhibition did not completely block protein synthesis. Much of the B cell protein landscape is not regulated by either mTORC1 or MYC; B cells still increased their cellular protein content during mTORC1 and MYC inhibition. This highlights that the regulatory pathways for protein synthesis and cell growth are complex, and additional hubs are likely to be important.

Iron has been widely shown to be essential for immune cell function. In B cells, iron availability is required for proliferation and antibody responses.[83,84] Our findings show that mTORC1 activity, SLC7A5 expression and MYC activity all regulate CD71 expression during B cell activation. We questioned whether mTORC1- and MYC-mediated proteome remodeling could in large part be attributed to iron availability. Indeed, chelating iron during B cell activation impaired B cell growth and protein synthesis. Our data support iron availability as an important component of the metabolic program that sustains B cell activation.

In conclusion, this study provides in-depth proteomic maps of naive and activated B cells and the impact of modulating key signaling pathways during B cell activation. These data provide new insights into the control of protein synthesis and cell growth in B cells and the machinery that drives B cell activation.

Limitations of the study

This study provides an in-depth analysis of B cell proteome remodeling in response to immune stimulation. While new biological insights have been provided, including the identification of shared and unique features of mTORC1 and MYC inhibition and the comparison of stimulation conditions, these experiments were performed by culturing primary cells *in vitro*. Future studies could explore the B cell protein landscape in immune-challenged mice and dissect B cell subpopulations, including those within the germinal center. In addition, this study examined B cell activation in mixed cell cultures from dissociated lymph nodes or spleens. This approach was chosen to limit disturbing cells before stimulation; however, activation and proteome remodeling may be impacted by the activity of other cells within the cell culture. Lastly, this study used rapamycin to block mTORC1 activity. Prolonged exposure to rapamycin may also impact the activity of mTORC2,[85] and this should be considered when interpreting results.

RESOURCE AVAILABILITY

Lead contact

Requests for further information and resources should be directed to and will be fulfilled by the lead contact, Andrew J.M. Howden (a.howden@dundee.ac.uk).

Materials availability

This study did not generate new unique reagents.

Data and code availability

Data

- All proteomics data are provided in file Data S1. Raw mass spectrometry data files and analysis files for proteomics data are publicly available from the PRoteomics IDEntifications Database (PRIDE), part of the ProteomeXchange data repository (https://www.ebi.ac.uk/pride/) and can be accessed with the following identifier's: PXD056624 for naive and activated B cell data ± rapamycin; PXD057711 for activated B cell data ± MYCi361; PXD070254 for individual and combined B cell stimuli and PXD074535 for *Myc* knockout data. Accession numbers are also listed in the key resources table. Our proteomics data (with the exception of the *Myc* KO data) are freely available and easy to explore on the Immunological Proteome Resource[86] www.immpres.co.uk. Flow cytometry data reported in this paper will be shared by the lead contact upon request.

Code

- This paper does not report original code.

Other items

- Any additional information required to reanalyze the data reported in this paper are available from the lead contact upon request.

ACKNOWLEDGMENTS

The authors would like to thank the University of Dundee flow cytometry facility for cell sorting support and the University of Dundee Biological Resource Unit. We sincerely thank K. Rajewsky, Mouse Genetics Cologne (MGC) Foundation, and A. Trumpp, German Cancer Research Center, Heidelberg, for sharing mouse models for *Myc* knockout experiments. We also thank Doreen Cantrell, Dana Cheung, and Simon Arthur for helpful discussions. Animations were drawn using BioRender. This research was supported by Wellcome Trust grants 205023/Z/16/Z and 227383/Z/23/Z and a Wellcome Trust Equipment Award, 202950/Z/16/Z. N.L. was supported by a PhD studentship funded by the Wellcome Trust doctoral training program (118787/Q/2213) while A.A.C.B. was supported by a PhD studentship funded by Medical Research Scotland (PHD-50637–2023).

AUTHOR CONTRIBUTIONS

A.J.M.H., N.L., H.K., M.P., and L.V.S. performed experiments. A.J.M.H., L.V.S., H.K., G.G., and F.S. designed experiments. O.J.J., L.V.S., N.L., A.A.C.B., A.J.B., and A.J.M.H. analyzed data. L.V.S., O.J.J., and A.J.M.H. wrote the manuscript. All authors read and commented on the manuscript. A.J.M.H. conceived the project.

DECLARATION OF INTERESTS

The authors declare no competing interests.

STAR★METHODS

Detailed methods are provided in the online version of this paper and include the following:

- KEY RESOURCES TABLE
- EXPERIMENTAL MODEL AND STUDY PARTICIPANT DETAILS
  - Mice
- METHOD DETAILS
  - Culturing B cells and cell sorting
  - Flow cytometry assays for system-L amino acid uptake and protein synthesis
  - Proteomics sample preparation and peptide fractionation
  - Liquid chromatography mass spectrometry analysis (LC- MS/MS)
  - Proteomics data processing and analysis
- QUANTIFICATION AND STATISTICAL ANALYSIS

SUPPLEMENTAL INFORMATION

Supplemental information can be found online at https://doi.org/10.1016/j.isci.2026.118146.

Received: April 27, 2026
Revised: August 10, 2026
Accepted: October 21, 2026

REFERENCES

1. Shen, P., and Fillatreau, S. (2015). Antibody-independent functions of B cells: a focus on cytokines. Nat. Rev. Immunol. *15*, 441–451. https://doi.org/10.1038/nri3857.
2. Nutt, S.L., Hodgkin, P.D., Tarlinton, D.M., and Corcoran, L.M. (2015). The generation of antibody-secreting plasma cells. Nat. Rev. Immunol. *15*, 160–171. https://doi.org/10.1038/nri3795.
3. Bashford-Rogers, R.J.M., Bergamaschi, L., McKinney, E.F., Pombal, D.C., Mescia, F., Lee, J.C., Thomas, D.C., Flint, S.M., Kellam, P., Jayne, D.R.W., et al. (2019). Analysis of the B cell receptor repertoire in six immune-mediated diseases. Nature *574*, 122–126. https://doi.org/10.1038/s41586-019-1595-3.
4. Jain, R.W., and Yong, V.W. (2022). B cells in central nervous system disease: diversity, locations and pathophysiology. Nat. Rev. Immunol. *22*, 513–524. https://doi.org/10.1038/s41577-021-00652-6.
5. Sehn, L.H., and Salles, G. (2021). Diffuse Large B-Cell Lymphoma. N. Engl. J. Med. *384*, 842–858. https://doi.org/10.1056/nejmra2027612.
6. Luo, W., Weisel, F., and Shlomchik, M.J. (2018). B Cell Receptor and CD40 Signaling Are Rewired for Synergistic Induction of the c-Myc Transcription Factor in Germinal Center B Cells. Immunity *48*, 313–326.e5. https://doi.org/10.1016/j.immuni.2018.01.008.
7. Lebman, D.A., and Coffman, R.L. (1988). Interleukin 4 causes isotype switching to IgE in T cell-stimulated clonal B cell cultures. J. Exp. Med. *168*, 853–862. https://doi.org/10.1084/jem.168.3.853.
8. Duan, L., Liu, D., Chen, H., Mintz, M.A., Chou, M.Y., Kotov, D.I., Xu, Y., An, J., Laidlaw, B.J., and Cyster, J.G. (2021). Follicular dendritic cells restrict interleukin-4 availability in germinal centers and foster memory B cell generation. Immunity *54*, 2256–2272.e6. https://doi.org/10.1016/j.immuni.2021.08.028.
9. Shehata, L., Thouvenel, C.D., Hondowicz, B.D., Pew, L.A., Pritchard, G.H., Rawlings, D.J., Choi, J., and Pepper, M. (2024). Interleukin 4 downregulates transcription factor BCL6 to promote memory B cell selection in germinal centers. Immunity *57*, 843–858.e5. https://doi.org/10.1016/j.immuni.2024.02.018.
10. Fowler, T., Garruss, A.S., Ghosh, A., De, S., Becker, K.G., Wood, W.H., Weirauch, M.T., Smale, S.T., Aronow, B., Sen, R., et al. (2015). Divergence of transcriptional landscape occurs early in B cell activation. Epigenetics Chromatin *8*, 20. https://doi.org/10.1186/s13072-015-0012-x.
11. Huang, H., Narayanan, H.V., Xiang, M.Y., Kesarwani, V., and Hoffmann, A. (2025). Synergy and antagonism in the integration of BCR and CD40 signals that control B-cell population expansion. Mol. Syst. Biol. *21*, 1119–1146. https://doi.org/10.1038/s44320-025-00124-2.
12. Haxhinasto, S.A., and Bishop, G.A. (2004). Synergistic B Cell Activation by CD40 and the B Cell Antigen Receptor. J. Biol. Chem. *279*, 2575–2582. https://doi.org/10.1074/jbc.m310628200.
13. Tellier, J., Shi, W., Minnich, M., Liao, Y., Crawford, S., Smyth, G.K., Kallies, A., Busslinger, M., and Nutt, S.L. (2016). Blimp-1 controls plasma cell function through regulation of immunoglobulin secretion and the unfolded protein response. Nat. Immunol. *17*, 323–330. https://doi.org/10.1038/ni.3348.
14. Waters, L.R., Ahsan, F.M., Wolf, D.M., Shirihai, O., and Teitell, M.A. (2018). Initial B Cell Activation Induces Metabolic Reprogramming and Mitochondrial Remodeling. iScience *5*, 99–109. https://doi.org/10.1016/j.isci.2018.07.005.
15. Shi, W., Liao, Y., Willis, S.N., Taubenheim, N., Inouye, M., Tarlinton, D.M., Smyth, G.K., Hodgkin, P.D., Nutt, S.L., and Corcoran, L.M. (2015). Transcriptional profiling of mouse B cell terminal differentiation defines a signature for antibody-secreting plasma cells. Nat. Immunol. *16*, 663–673. https://doi.org/10.1038/ni.3154.
16. Boothby, M., and Rickert, R.C. (2017). Metabolic Regulation of the Immune Humoral Response. Immunity *46*, 743–755. https://doi.org/10.1016/j.immuni.2017.04.009.
17. Caro-Maldonado, A., Wang, R., Nichols, A.G., Kuraoka, M., Milasta, S., Sun, L.D., Gavin, A.L., Abel, E.D., Kelsoe, G., Green, D.R., et al. (2014). Metabolic Reprogramming Is Required for Antibody Production That Is Suppressed in Anergic but Exaggerated in Chronically BAFF-Exposed B Cells. J. Immunol. *192*, 3626–3636. https://doi.org/10.4049/jimmunol.1302062.
18. Liu, G.Y., and Sabatini, D.M. (2020). mTOR at the nexus of nutrition, growth, ageing and disease. Nat. Rev. Mol. Cell Biol. *21*, 183–203. https://doi.org/10.1038/s41580-019-0199-y.
19. Raybuck, A.L., Cho, S.H., Li, J., Rogers, M.C., Lee, K., Williams, C.L., Shlomchik, M., Thomas, J.W., Chen, J., Williams, J.V., et al. (2018). B Cell–Intrinsic mTORC1 Promotes Germinal Center–Defining Transcription Factor Gene Expression, Somatic Hypermutation, and Memory B Cell Generation in Humoral Immunity. J. Immunol. *200*, 2627–2639. https://doi.org/10.4049/jimmunol.1701321.
20. Iwata, T.N., Ramírez, J.A., Tsang, M., Park, H., Margineantu, D.H., Hockenbery, D.M., and Iritani, B.M. (2016). Conditional Disruption of Raptor Reveals an Essential Role for mTORC1 in B Cell Development, Survival, and Metabolism. J. Immunol. *197*, 2250–2260. https://doi.org/10.4049/jimmunol.1600492.
21. Zhang, S., Readinger, J.A., DuBois, W., Janka-Junttila, M., Robinson, R., Pruitt, M., Bliskovsky, V., Wu, J.Z., Sakakibara, K., Patel, J., et al. (2011). Constitutive reductions in mTOR alter cell size, immune cell development, and antibody production. Blood *117*, 1228–1238. https://doi.org/10.1182/blood-2010-05-287821.
22. Iwata, T.N., Ramírez-Komo, J.A., Park, H., and Iritani, B.M. (2017). Control of B lymphocyte development and functions by the mTOR signaling pathways. Cytokine Growth Factor Rev. *35*, 47–62. https://doi.org/10.1016/j.cytogfr.2017.04.005.
23. Gaudette, B.T., Jones, D.D., Bortnick, A., Argon, Y., and Allman, D. (2020). mTORC1 coordinates an immediate unfolded protein response-related transcriptome in activated B cells preceding antibody secretion. Nat. Commun. *11*, 723. https://doi.org/10.1038/s41467-019-14032-1.
24. Tan, H., Yang, K., Li, Y., Shaw, T.I., Wang, Y., Blanco, D.B., Wang, X., Cho, J.-H., Wang, H., Rankin, S., et al. (2017). Integrative Proteomics and Phosphoproteomics Profiling Reveals Dynamic Signaling Networks and Bioenergetics Pathways Underlying T Cell Activation. Immunity *46*, 488–503. https://doi.org/10.1016/j.immuni.2017.02.010.
25. Rieckmann, J.C., Geiger, R., Hornburg, D., Wolf, T., Kveler, K., Jarrossay, D., Sallusto, F., Shen-Orr, S.S., Lanzavecchia, A., Mann, M., et al. (2017). Social network architecture of human immune cells unveiled by quantitative proteomics. Nat. Immunol. *18*, 583–593. https://doi.org/10.1038/ni.3693.
26. Salerno, F., Howden, A.J.M., Matheson, L.S., Gizlenci, Ö., Screen, M., Lingel, H., Brunner-Weinzierl, M.C., and Turner, M. (2023). An integrated proteome and transcriptome of B cell maturation defines poised activation states of transitional and mature B cells. Nat. Commun. *14*, 5116. https://doi.org/10.1038/s41467-023-40621-2.
27. Hukelmann, J.L., Anderson, K.E., Sinclair, L.V., Grzes, K.M., Murillo, A.B., Hawkins, P.T., Stephens, L.R., Lamond, A.I., and Cantrell, D.A. (2016). The cytotoxic T cell proteome and its shaping by the kinase mTOR. Nat. Immunol. *17*, 104–112. https://doi.org/10.1038/ni.3314.
28. Wiśniewski, J.R., Hein, M.Y., Cox, J., and Mann, M. (2014). A "Proteomic Ruler" for Protein Copy Number and Concentration Estimation without Spike-in Standards. Mol. Cell. Proteomics *13*, 3497–3506. https://doi.org/10.1074/mcp.m113.037309.
29. Winkelmann, R., Sandrock, L., Kirberg, J., Jäck, H.-M., and Schuh, W. (2014). KLF2– A Negative Regulator of Pre-B Cell Clonal Expansion and B Cell Activation. PLoS One *9*, e97953. https://doi.org/10.1371/journal.pone.0097953.
30. Hart, G.T., Wang, X., Hogquist, K.A., and Jameson, S.C. (2011). Krüppel-like factor 2 (KLF2) regulates B-cell reactivity, subset differentiation, and trafficking molecule expression. Proc. Natl. Acad. Sci. USA *108*, 716–721. https://doi.org/10.1073/pnas.1013168108.

31. Wittner, J., and Schuh, W. (2023). Krüppel-like factor 2: a central regulator of B cell differentiation and plasma cell homing. Front. Immunol. *14*, 1172641. https://doi.org/10.3389/fimmu.2023.1172641.

32. Suzuki, C., Garces, R.G., Edmonds, K.A., Hiller, S., Hyberts, S.G., Marintchev, A., and Wagner, G. (2008). PDCD4 inhibits translation initiation by binding to eIF4A using both its MA3 domains. Proc. Natl. Acad. Sci. USA *105*, 3274–3279. https://doi.org/10.1073/pnas.0712235105.

33. Loh, P.G., Yang, H.S., Walsh, M.A., Wang, Q., Wang, X., Cheng, Z., Liu, D., and Song, H. (2009). Structural basis for translational inhibition by the tumour suppressor Pdcd4. EMBO J. *28*, 274–285. https://doi.org/10.1038/emboj.2008.278.

34. Kashiwada, M., Levy, D.M., McKeag, L., Murray, K., Schröder, A.J., Canfield, S.M., Traver, G., and Rothman, P.B. (2010). IL-4-induced transcription factor NFIL3/E4BP4 controls IgE class switching. Proc. Natl. Acad. Sci. USA *107*, 821–826. https://doi.org/10.1073/pnas.0909235107.

35. Li, S., Miao, T., Sebastian, M., Bhullar, P., Ghaffari, E., Liu, M., Symonds, A.L.J., and Wang, P. (2012). The Transcription Factors Egr2 and Egr3 Are Essential for the Control of Inflammation and Antigen-Induced Proliferation of B and T Cells. Immunity *37*, 685–696. https://doi.org/10.1016/j.immuni.2012.08.001.

36. Cobaleda, C., Schebesta, A., Delogu, A., and Busslinger, M. (2007). Pax5: the guardian of B cell identity and function. Nat. Immunol. *8*, 463–470. https://doi.org/10.1038/ni1454.

37. Fedl, A.S., Tagoh, H., Gruenbacher, S., Sun, Q., Schenk, R.L., Froussios, K., Jaritz, M., Busslinger, M., and Schwickert, T.A. (2024). Transcriptional function of E2A, Ebf1, Pax5, Ikaros and Aiolos analyzed by in vivo acute protein degradation in early B cell development. Nat. Immunol. *25*, 1663–1677. https://doi.org/10.1038/s41590-024-01933-7.

38. Scalise, M., Pochini, L., Console, L., Losso, M.A., and Indiveri, C. (2018). The Human SLC1A5 (ASCT2) Amino Acid Transporter: From Function to Structure and Role in Cell Biology. Front. Cell Dev. Biol. *6*, 96. https://doi.org/10.3389/fcell.2018.00096.

39. Kanai, Y., Segawa, H., Miyamoto, K.I., Uchino, H., Takeda, E., and Endou, H. (1998). Expression Cloning and Characterization of a Transporter for Large Neutral Amino Acids Activated by the Heavy Chain of 4F2 Antigen (CD98). J. Biol. Chem. *273*, 23629–23632. https://doi.org/10.1074/jbc.273.37.23629.

40. Rath, S., Sharma, R., Gupta, R., Ast, T., Chan, C., Durham, T.J., Goodman, R.P., Grabarek, Z., Haas, M.E., Hung, W.H.W., et al. (2021). MitoCarta3.0: an updated mitochondrial proteome now with sub-organelle localization and pathway annotations. Nucleic Acids Res. *49*, D1541–D1547. https://doi.org/10.1093/nar/gkaa1011.

41. Sinclair, L.V., Rolf, J., Emslie, E., Shi, Y.-B., Taylor, P.M., and Cantrell, D.A. (2013). Control of amino-acid transport by antigen receptors coordinates the metabolic reprogramming essential for T cell differentiation. Nat. Immunol. *14*, 500–508. https://doi.org/10.1038/ni.2556.

42. Sinclair, L.V., Howden, A.J.M., Brenes, A., Spinelli, L., Hukelmann, J.L., Macintyre, A.N., Liu, X., Thomson, S., Taylor, P.M., Rathmell, J.C., et al. (2019). Antigen receptor control of methionine metabolism in T cells. eLife *8*, e44210. https://doi.org/10.7554/elife.44210.

43. Palacín, M., and Kanai, Y. (2004). The ancillary proteins of HATs: SLC3 family of amino acid transporters. Pflügers Arch. *447*, 490–494. https://doi.org/10.1007/s00424-003-1062-7.

44. Jabara, H.H., Boyden, S.E., Chou, J., Ramesh, N., Massaad, M.J., Benson, H., Bainter, W., Fraulino, D., Rahimov, F., Sieff, C., et al. (2016). A missense mutation in TFRC, encoding transferrin receptor 1, causes combined immunodeficiency. Nat. Genet. *48*, 74–78. https://doi.org/10.1038/ng.3465.

45. Neckers, L.M., Yenokida, G., and James, S.P. (1984). The role of the transferrin receptor in human B lymphocyte activation. J. Immunol. *133*, 2437–2441.

46. Frost, J.N., Tan, T.K., Abbas, M., Wideman, S.K., Bonadonna, M., Stoffel, N.U., Wray, K., Kronsteiner, B., Smits, G., Campagna, D.R., et al. (2021). Hepcidin-Mediated Hypoferremia Disrupts Immune Responses to Vaccination and Infection. Med *2*, 164–179.e12. https://doi.org/10.1016/j.medj.2020.10.004.

47. Tanner, L.B., Goglia, A.G., Wei, M.H., Sehgal, T., Parsons, L.R., Park, J.O., White, E., Toettcher, J.E., and Rabinowitz, J.D. (2018). Four Key Steps Control Glycolytic Flux in Mammalian Cells. Cell Syst. *7*, 49–62.e8. https://doi.org/10.1016/j.cels.2018.06.003.

48. Yazicioglu, Y.F., Marin, E., Sandhu, C., Galiani, S., Raza, I.G.A., Ali, M., Kronsteiner, B., Compeer, E.B., Attar, M., Dunachie, S.J., et al. (2023). Dynamic mitochondrial transcription and translation in B cells control germinal center entry and lymphomagenesis. Nat. Immunol. *24*, 991–1006. https://doi.org/10.1038/s41590-023-01484-3.

49. Iborra-Pernichi, M., García, J.R., Esperanza, M.V. de la, Estrada, B.S., Bovolenta, E.R., Cifuentes, C., Carro, C.P., Martínez, T.G., García-Consuegra, J., Rey-Stolle, M.F., et al. (2024). Defective mitochondria remodelling in B cells leads to an aged immune response. Nat. Commun. *15*, 2569. https://doi.org/10.1038/s41467-024-46763-1.

50. Teh, M.R., Frost, J.N., Armitage, A.E., and Drakesmith, H. (2021). Analysis of Iron and Iron-Interacting Protein Dynamics During T-Cell Activation. Front. Immunol. *12*, 714613. https://doi.org/10.3389/fimmu.2021.714613.

51. Inabe, K., Ishiai, M., Scharenberg, A.M., Freshney, N., Downward, J., and Kurosaki, T. (2002). Vav3 Modulates B Cell Receptor Responses by Regulating Phosphoinositide 3-Kinase Activation. J. Exp. Med. *195*, 189–200. https://doi.org/10.1084/jem.20011571.

52. Vaidyanathan, B., Chaudhry, A., Yewdell, W.T., Angeletti, D., Yen, W.-F., Wheatley, A.K., Bradfield, C.A., McDermott, A.B., Yewdell, J.W., Rudensky, A.Y., et al. (2017). The aryl hydrocarbon receptor controls cell-fate decisions in B cells. J. Exp. Med. *214*, 197–208. https://doi.org/10.1084/jem.20160789.

53. Muto, A., Ochiai, K., Kimura, Y., Itoh-Nakadai, A., Calame, K.L., Ikebe, D., Tashiro, S., and Igarashi, K. (2010). Bach2 represses plasma cell gene regulatory network in B cells to promote antibody class switch. EMBO J. *29*, 4048–4061. https://doi.org/10.1038/emboj.2010.257.

54. Klemsz, M.J., Justement, L.B., Palmer, E., and Cambier, J.C. (1989). Induction of c-fos and c-myc expression during B cell activation by IL-4 and immunoglobulin binding ligands. J. Immunol. *143*, 1032–1039.

55. Steach, H.R., York, A.G., Skadow, M.H., Chen, S., Zhao, J., Williams, K.J., Zhou, Q., Hsieh, W.-Y., Brewer, J.R., Qu, R., et al. (2024). IL-4 Licenses B Cell Activation Through Cholesterol Synthesis. bioRxiv, 2024.05.13.593964. https://doi.org/10.1101/2024.05.13.593964.

56. Marchingo, J.M., Sinclair, L.V., Howden, A.J., and Cantrell, D.A. (2020). Quantitative analysis of how Myc controls T cell proteomes and metabolic pathways during T cell activation. eLife *9*, e53725. https://doi.org/10.7554/elife.53725.

57. Howden, A.J.M., Hukelmann, J.L., Brenes, A., Spinelli, L., Sinclair, L.V., Lamond, A.I., and Cantrell, D.A. (2019). Quantitative analysis of T cell proteomes and environmental sensors during T cell differentiation. Nat. Immunol. *20*, 1542–1554. https://doi.org/10.1038/s41590-019-0495-x.

58. Chi, H. (2012). Regulation and function of mTOR signalling in T cell fate decisions. Nat. Rev. Immunol. *12*, 325–338. https://doi.org/10.1038/nri3198.

59. Pollizzi, K.N., and Powell, J.D. (2015). Regulation of T cells by mTOR: the known knowns and the known unknowns. Trends Immunol. *36*, 13–20. https://doi.org/10.1016/j.it.2014.11.005.

60. Goul, C., Peruzzo, R., and Zoncu, R. (2023). The molecular basis of nutrient sensing and signalling by mTORC1 in metabolism regulation and disease. Nat. Rev. Mol. Cell Biol. *24*, 857–875. https://doi.org/10.1038/s41580-023-00641-8.

61. Hawkins, E.D., Markham, J.F., McGuinness, L.P., and Hodgkin, P.D. (2009). A single-cell pedigree analysis of alternative stochastic lymphocyte fates. Proc. Natl. Acad. Sci. USA *106*, 13457–13462. https://doi.org/10.1073/pnas.0905629106.

62. Turner, M.L., Hawkins, E.D., and Hodgkin, P.D. (2008). Quantitative Regulation of B Cell Division Destiny by Signal Strength. J. Immunol. *181*, 374–382. https://doi.org/10.4049/jimmunol.181.1.374.

63. Patterson, D.G., Kania, A.K., Price, M.J., Rose, J.R., Scharer, C.D., and Boss, J.M. (2021). An IRF4–MYC–mTORC1 Integrated Pathway Controls Cell Growth and the Proliferative Capacity of Activated B Cells during B Cell Differentiation In Vivo. J. Immunol. *207*, 1798–1811. https://doi.org/10.4049/jimmunol.2100440.

64. Wang, H., Lee, C.H., Qi, C., Tailor, P., Feng, J., Abbasi, S., Atsumi, T., and Morse, H.C. (2008). IRF8 regulates B-cell lineage specification, commitment, and differentiation. Blood *112*, 4028–4038. https://doi.org/10.1182/blood-2008-01-129049.

65. Lee, C.H., Melchers, M., Wang, H., Torrey, T.A., Slota, R., Qi, C.-F., Kim, J.Y., Lugar, P., Kong, H.J., Farrington, L., et al. (2006). Regulation of the germinal center gene program by interferon (IFN) regulatory factor 8/IFN consensus sequence-binding protein. J. Exp. Med. *203*, 63–72. https://doi.org/10.1084/jem.20051450.

66. Wang, H., Jain, S., Li, P., Lin, J.-X., Oh, J., Qi, C., Gao, Y., Sun, J., Sakai, T., Naghashfar, Z., et al. (2019). Transcription factors IRF8 and PU.1 are required for follicular B cell development and BCL6-driven germinal center responses. Proc. Natl. Acad. Sci. USA *116*, 9511–9520. https://doi.org/10.1073/pnas.1901258116.

67. Villa, M., Gialitakis, M., Tolaini, M., Ahlfors, H., Henderson, C.J., Wolf, C.R., Brink, R., and Stockinger, B. (2017). Aryl hydrocarbon receptor is required for optimal B-cell proliferation. EMBO J. *36*, 116–128. https://doi.org/10.15252/embj.201695027.

68. Sinclair, L.V., Neyens, D., Ramsay, G., Taylor, P.M., and Cantrell, D.A. (2018). Single cell analysis of kynurenine and System L amino acid transport in T cells. Nat. Commun. *9*, 1981. https://doi.org/10.1038/s41467-018-04366-7.

69. Nie, Z., Hu, G., Wei, G., Cui, K., Yamane, A., Resch, W., Wang, R., Green, D.R., Tessarollo, L., Casellas, R., et al. (2012). c-Myc Is a Universal Amplifier of Expressed Genes in Lymphocytes and Embryonic Stem Cells. Cell *151*, 68–79. https://doi.org/10.1016/j.cell.2012.08.033.

70. Han, H., Jain, A.D., Truica, M.I., Izquierdo-Ferrer, J., Anker, J.F., Lysy, B., Sagar, V., Luan, Y., Chalmers, Z.R., Unno, K., et al. (2019). Small-Molecule MYC Inhibitors Suppress Tumor Growth and Enhance Immunotherapy. Cancer Cell *36*, 483–497.e15. https://doi.org/10.1016/j.ccell.2019.10.001.

71. Preston, G.C., Sinclair, L.V., Kaskar, A., Hukelmann, J.L., Navarro, M.N., Ferrero, I., MacDonald, H.R., Cowling, V.H., and Cantrell, D.A. (2015). Single cell tuning of Myc expression by antigen receptor signal strength and interleukin-2 in T lymphocytes. EMBO J. *34*, 2008–2024. https://doi.org/10.15252/embj.201490252.

72. O'Donnell, K.A., Yu, D., Zeller, K.I., Kim, J.W., Racke, F., Thomas-Tikhonenko, A., and Dang, C.V. (2006). Activation of Transferrin Receptor 1 by c-Myc Enhances Cellular Proliferation and Tumorigenesis. Mol. Cell Biol. *26*, 2373–2386. https://doi.org/10.1128/mcb.26.6.2373-2386.2006.

73. Sun, Y., Wen, J., Xu, T., and Meng, L. (2023). Reduction of peritoneal cavity B1a cells in adult Slc7a5 knockdown mice via dysregulating the mTOR pathway. Int. Immunopharmacol. *117*, 109939. https://doi.org/10.1016/j.intimp.2023.109939.

74. Torigoe, M., Maeshima, K., Ozaki, T., Omura, Y., Gotoh, K., Tanaka, Y., Ishii, K., and Shibata, H. (2019). l-Leucine influx through Slc7a5 regulates inflammatory responses of human B cells via mammalian target of rapamycin complex 1 signaling. Mod. Rheumatol. *29*, 885–891. https://doi.org/10.1080/14397595.2018.1510822.

75. Cantor, J., Browne, C.D., Ruppert, R., Féral, C.C., Fässler, R., Rickert, R.C., and Ginsberg, M.H. (2009). CD98hc facilitates B cell proliferation and adaptive humoral immunity. Nat. Immunol. *10*, 412–419. https://doi.org/10.1038/ni.1712.

76. Cheung, D.M.S., Razsolkov, M., Bonacina, F., Andrews, S., Sumoreeah, M., Sinclair, L.V., Howden, A.J.M., and Arthur, J.S.C. (2026). Lipopolysaccharide stimulates dynamic changes in B cell metabolism to promote proliferation. eLife. https://doi.org/10.7554/eLife.109093.3.

77. Ben-Sahra, I., and Manning, B.D. (2017). mTORC1 signaling and the metabolic control of cell growth. Curr. Opin. Cell Biol. *45*, 72–82. https://doi.org/10.1016/j.ceb.2017.02.012.

78. Valvezan, A.J., and Manning, B.D. (2019). Molecular logic of mTORC1 signalling as a metabolic rheostat. Nat. Metab. *1*, 321–333. https://doi.org/10.1038/s42255-019-0038-7.

79. Jones, D.D., Gaudette, B.T., Wilmore, J.R., Chernova, I., Bortnick, A., Weiss, B.M., and Allman, D. (2016). mTOR has distinct functions in generating versus sustaining humoral immunity. J. Clin. Investig. *126*, 4250–4261. https://doi.org/10.1172/jci86504.

80. Benhamron, S., Pattanayak, S.P., Berger, M., and Tirosh, B. (2015). mTOR Activation Promotes Plasma Cell Differentiation and Bypasses XBP-1 for Immunoglobulin Secretion. Mol. Cell Biol. *35*, 153–166. https://doi.org/10.1128/mcb.01187-14.

81. Zeng, H., Yu, M., Tan, H., Li, Y., Su, W., Shi, H., Dhungana, Y., Guy, C., Neale, G., Cloer, C., et al. (2018). Discrete roles and bifurcation of PTEN signaling and mTORC1-mediated anabolic metabolism underlie IL-7–driven B lymphopoiesis. Sci. Adv. *4*, eaar5701. https://doi.org/10.1126/sciadv.aar5701.

82. de Alboran, I.M., O'Hagan, R.C., Gärtner, F., Malynn, B., Davidson, L., Rickert, R., Rajewsky, K., DePinho, R.A., and Alt, F.W. (2001). Analysis of C-MYC Function in Normal Cells via Conditional Gene-Targeted Mutation. Immunity *14*, 45–55. https://doi.org/10.1016/s1074-7613(01)00088-7.

83. Ned, R.M., Swat, W., and Andrews, N.C. (2003). Transferrin receptor 1 is differentially required in lymphocyte development. Blood *102*, 3711–3718. https://doi.org/10.1182/blood-2003-04-1086.

84. Stoffel, N.U., and Drakesmith, H. (2024). Effects of Iron Status on Adaptive Immunity and Vaccine Efficacy: A Review. Adv. Nutr. *15*, 100238. https://doi.org/10.1016/j.advnut.2024.100238.

85. Sarbassov, D.D., Ali, S.M., Sengupta, S., Sheen, J.-H., Hsu, P.P., Bagley, A.F., Markhard, A.L., and Sabatini, D.M. (2006). Prolonged Rapamycin Treatment Inhibits mTORC2 Assembly and Akt/PKB. Mol. Cell *22*, 159–168. https://doi.org/10.1016/j.molcel.2006.03.029.

86. Brenes, A.J., Lamond, A.I., and Cantrell, D.A. (2023). The Immunological Proteome Resource. Nat. Immunol. *24*, 731. https://doi.org/10.1038/s41590-023-01483-4.

87. Rickert, R.C., Rajewsky, K., and Roes, J. (1995). Impairment of T-cell-dependent B-cell responses and B-1 cell development in CD19-deficient mice. Nature *376*, 352–355. https://doi.org/10.1038/376352a0.

88. Trumpp, A., Refaeli, Y., Oskarsson, T., Gasser, S., Murphy, M., Martin, G.R., and Bishop, J.M. (2001). c-Myc regulates mammalian body size by controlling cell number but not cell size. Nature *414*, 768–773. https://doi.org/10.1038/414768a.

89. Rappsilber, J., Mann, M., and Ishihama, Y. (2007). Protocol for micro-purification, enrichment, pre-fractionation and storage of peptides for proteomics using StageTips. Nat. Protoc. *2*, 1896–1906. https://doi.org/10.1038/nprot.2007.261.

90. Molina-Gonzalez, I., Holloway, R.K., Jiwaji, Z., Dando, O., Kent, S.A., Emelianova, K., Lloyd, A.F., Forbes, L.H., Mahmood, A., Skripuletz, T., et al. (2023). Astrocyte-oligodendrocyte interaction regulates central nervous system regeneration. Nat. Commun. *14*, 3372. https://doi.org/10.1038/s41467-023-39046-8.

91. Walgrave, H., Penning, A., Tosoni, G., Snoeck, S., Davie, K., Davis, E., Wolfs, L., Sierksma, A., Mars, M., Bu, T., et al. (2023). microRNA-132 regulates gene expression programs involved in microglial homeostasis. iScience *26*, 106829. https://doi.org/10.1016/j.isci.2023.106829.

92. Sollberger, G., Brenes, A.J., Warner, J., Arthur, J.S.C., and Howden, A.J.M. (2024). Quantitative proteomics reveals tissue-specific, infection-induced and species-specific neutrophil protein signatures. Sci. Rep. *14*, 5966. https://doi.org/10.1038/s41598-024-56163-6.

93. Cox, J., and Mann, M. (2008). MaxQuant enables high peptide identification rates, individualized p.p.b.-range mass accuracies and proteome-wide protein quantification. Nat. Biotechnol. *26*, 1367–1372. https://doi.org/10.1038/nbt.1511.

94. Tyanova, S., Temu, T., Sinitcyn, P., Carlson, A., Hein, M.Y., Geiger, T., Mann, M., and Cox, J. (2016). The Perseus computational platform for comprehensive analysis of (prote)omics data. Nat. Methods *13*, 731–740. https://doi.org/10.1038/nmeth.3901.

95. Ritchie, M.E., Phipson, B., Wu, D., Hu, Y., Law, C.W., Shi, W., and Smyth, G.K. (2015). limma powers differential expression analyses for RNA-sequencing and microarray studies. Nucleic Acids Res. *43*, e47. https://doi.org/10.1093/nar/gkv007.

STAR★METHODS

KEY RESOURCES TABLE

REAGENT or RESOURCE	SOURCE	IDENTIFIER
Antibodies		
Anti-mouse CD19 PE/Cyanine7	Biolegend	Cat#115520; RRID: AB_313655
Anti-mouse/human CD45R/B220 Brilliant violet 605 Clone: RA3-6B2	Biolegend	Cat#103243; RRID: AB_11203907
Anti-mouse CD93 (AA4.1, early B lineage) APC Clone: AA4.1	Biolegend	Cat#136510; RRID: AB_2275868
Anti-mouse CD21/35 (CR2/CR1) Pacific Blue Clone: 7E9	Biolegend	Cat#123414; RRID: AB_2085158
Anti-mouse CD23 APC/Cyanine7 Clone: B3B4	Biolegend	Cat#101630; RRID: AB_2571987
Anti-mouse CD19 APC/Cyanine7 Clone:6D5	Biolegend	Cat#115530; RRID: AB_830707
Anti-mouse CD19 FITC Clone: 1D3/CD19	Biolegend	Cat#152404; RRID: AB_2629813
Rat Anti-Mouse CD19 APC Clone: 1D3	BD Pharmingen	Cat#550992; RRID: AB_398483
Purified Rat Anti-Mouse CD16/CD32 (Mouse BD Fc Block)	BD Pharmingen	Cat#553142; RRID: AB_394657
anti-IgM (AffiniPure F(ab')$_2$ fragment goat anti-mouse)	Jackson ImmunoResearch Laboratories Inc	Cat#115–006-075; RRID: AB_2338474
anti-CD40 (FGK4.5/FGK45 anti-mouse CD40)	BioXcell	Cat#BE0016-2; RRID: AB_1107647
Chemicals, peptides, and recombinant proteins		
MYCi361 (MYC inhibitor)	MedChem Express	Cat#HY-129600
Rapamycin (mTORC1 inhibitor)	Merck	Cat#R8781
Recombinant Murine IL-4	PeproTech	Cat#214–14
Lipopolysaccharide (LPS)	Merck	Cat#L2654
Deferiprone (3-Hydroxy-1,2-dimethyl-4(1H)-pyridone)	Merck	Cat#379409
L-Kynurenine	Merck	Cat#K8625
2-Amino-2-norbornanecarboxylic acid (BCH)	Merck	Cat#A7902
O-Propargyl-puromycin (OPP)	Jena Bioscience	Cat#NU-931
Deposited data		
Proteomics data for naive and activated B cells ± rapamycin	https://www.ebi.ac.uk/pride/	PRIDE: PXD056624
Proteomics data for activated B cell data ± MYCi361	https://www.ebi.ac.uk/pride/	PRIDE: PXD057711
Proteomics data for individual and combined B cell stimuli	https://www.ebi.ac.uk/pride/	PRIDE: PXD070254
Proteomics data for *Myc* KO B cells	https://www.ebi.ac.uk/pride/	PRIDE: PXD074535
Experimental models: Organisms/strains		
Wildtype C57BL6/J mice	Charles River	wildtype
Myc-eGFP mice	Nie et al.[69]	*Myc*-GFP
VavCre x *Slc7a5*$^{fl/fl}$	Sinclair et al.[41]	*Slc7a5* KO
CD19 Cre *Myc* - B6.129P2(C)-Cd19tm1(cre)Cgn/J x Myctm2.1Atp	Rickert et al.[87] and Trumpp et al.[88]	*Myc* KO
Software and algorithms		
MaxQuant version 1.6.10.43	MaxQuant	https://maxquant.org/

(*Continued on next page*)

Continued

REAGENT or RESOURCE	SOURCE	IDENTIFIER
Perseus version 1.6.6.0	MaxQuant	https://maxquant.net/perseus/
Spectronaut version 19	Biognosys	https://biognosys.com/software/spectronaut/
R	The R project for statistical computing	https://www.r-project.org/
Linear Models for Microarray and Omics Data (LIMMA)	Bioconductor	https://bioconductor.org/packages/release/bioc/html/limma.html
clusterProfiler	Bioconductor	https://bioconductor.org/packages/release/bioc/html/clusterProfiler.html
FlowJo software version 10	Waters Bioscience	https://www.flowjo.com/flowjo/overview
GraphPad Prism version 10	GraphPad	https://www.graphpad.com

EXPERIMENTAL MODEL AND STUDY PARTICIPANT DETAILS

Mice

Male wildtype C57BL/6 mice (Charles Rivers) aged between 8 and 12 weeks were used for proteomics experiments examining B cell stimuli and inhibitor treatments and for validation experiments examining protein synthesis, amino acid uptake and marker expression. Male and female *Myc*-eGFP mice[69] aged between 8 and 12 weeks were used to monitor MYC expression by flow cytometry. Male and female VavCre x *Slc7a5*$^{fl/fl}$ mice[41] aged between 8 and 12 weeks were used for *Slc7a5* KO experiments. All mice were maintained in the Biological Resource Unit at the University of Dundee using procedures approved by the University Ethical Review Committee and under the authorization of the UK Home Office Animals (Scientific Procedures) Act 1986 and under the ARRIVE 2.0 guidelines. *Slc7a5* KO experiments were performed under the animal licence 60/3812 while *Myc*-eGFP animal experiments were performed under the animal licence P4BD0CE74. Both licences were granted by the Animals in Science Regulation Unit, UK Home Office.

For proteomics experiments examining the impact of *Myc* knockout, *Myc*-floxed mice[88] were crossed to Cd19Cre[87] to generate Cd19Cre *Myc*$^{wt/wt}$ *and* Cd19Cre *Myc*$^{fl/fl}$ animals. 10–13 weeks old female mice were used for the experiment. All animal experiments were approved by the Veterinary Office regulations of the Cantone Ticino, Switzerland (authorisation number TI 42/2021), and all methods were performed in accordance with the Swiss guidelines and regulations.

METHOD DETAILS

Culturing B cells and cell sorting

For all experiments except *Myc* KO proteomics, cells were cultured at 37°C with 5% CO_2 in RPMI 1640 containing glutamine (Invitrogen) and supplemented with 10% FBS (Gibco), 50 μM β-mercaptoethanol (Sigma) and penicillin/streptomycin (Gibco). For all proteomic experiments examining B cell stimuli and inhibitor treatments (with the exception of the *Myc* KO proteomes) and for validation experiments examining protein synthesis, amino acid uptake and marker expression (with the exception of *Slc7a5* KO experiments) the following peripheral lymph nodes were used: cervical, axillary, brachial and inguinal. Lymph nodes were extracted from mice, mashed in RPMI media before filtering through a 70 μm cell strainer. For generating a pure population of naive B cells, lymphocytes were incubated with FC block and then stained with CD19 FITC, CD93 APC and DAPI. CD19^{+} and CD93^{-}live cells were sorted using a Sony LE-MA900. Sorted cells were washed twice with HBSS and snap frozen in liquid nitrogen and stored at −80°C until processing for mass spectrometry. For T dependent and T cell independent B cell activation, lymph nodes were macerated and the total pool of cells was suspended in RPMI at a final density of 1.5 million cells/ml and activated for 24 h in the presence of either 10 μg/mL anti-IgM (AffiniPure F(ab')$_2$ fragment goat anti-mouse) (Jackson ImmunoResearch), 10 μg/mL anti-CD40 (FGK4.5/FGK45 anti-mouse CD40) (BioXcell) and 10 ng/mL IL4 (PeproTech) or 20 μg/mL LPS (Merck) and 10 ng/mL IL4. For experiments exploring the synergistic impact of B cell stimuli, lymph nodes were macerated and the total pool of cells was suspended in RPMI at a final density of 1.5 million cells/ml and activated for 40 h in the presence of combinations of anti-IgM, anti-CD40 and IL4 at the above concentrations. For rapamycin treatment, cells were activated as described above for 24 h but in the presence of 20 nM rapamycin for the full duration of activation. For MYC inhibition, cells were activated as above in the presence of 5 μM MYCi361. For all proteomes, except *Myc* KO, cells were sorted after activation. Cells were FC blocked and stained with CD19 APC (for activation and rapamycin treated cells) or CD19 APC-Cy7 (for control and MYCi361 treated cells) and DAPI, and live B cells were sorted and collected as described above. Example gating strategies for cell sorting are provided in the following supplementary figures: B cells activated with anti-IgM + anti-CD40 + IL4 +/− rapamycin or LPS + IL4 (Figure S3), naive B cells (Figure S4), B cells activated ± the MYC inhibitor MYCi361

(Figure S5), B cells activated with IL4 alone, anti-CD40 alone or anti-IgM alone (Figure S6) and B cells activated with anti-CD40 and IL4, anti-IgM and IL4, anti-IgM and anti-CD40, or anti-IgM and anti-CD40 and IL4 (Figure S7).

For *Slc7a5* KO experiments, splenocytes were activated using 10 μg/mL anti-IgM and 10 μg/mL anti-CD40. For iron chelation experiments lymphocytes were activated for 24 h as described above but in the presence of deferiprone (3-Hydroxy-1,2-dimethyl-4(1H)-pyridone) at 10 μM, 50 μM, 100 μM and 300 μM. For flow cytometry analysis, samples were analyzed on either a Novocyte or LSR Fortessa flow cytometer.

For *Myc* KO proteomics, splenic follicular (FO) B cells were FACS-sorted (SORP FACSymphony S6, BD Biosciences) for $B220^{+}$/$CD19^{+}$/$CD93^{-}$/$CD23^{+}$/$CD21^{int}$ and seeded at a density of $2x10^{6}$/mL in complete medium (RPMI, 10% FBS, 1% Penicillin-Streptomycin, 1% MEM NEAA, 1% GlutaMAX, 1% Sodium pyruvate, 0.1% 2-mercaptoethanol, all from Gibco). Cells were activated by anti-IgM (Jackson ImmunoResearch), coated overnight at a concentration of 10 μg/mL, together with recombinant mouse IL4 (PeproTech) added to a concentration of 2 ng/mL and cultured at 37°C for 24 h. After stimulation, cells were harvested and washed twice with Hanks' Balanced Salt Solution (HBSS, Gibco). Cells were then centrifuged and dry pellets were snap frozen in liquid nitrogen and stored at −80°C prior to lysis for MS.

Flow cytometry assays for system-L amino acid uptake and protein synthesis

System-L amino acid uptake was measured using a single cell flow cytometry assay.[68] In brief, cervical, axillary, brachial and inguinal lymph nodes were extracted from wildtype mice, and B cells were activated ± rapamycin as described above. After 24 h of activation cells were surface stained and washed in pre-warmed HBSS and resuspended in 200 μL HBSS. Cells were treated with either an inhibitor of system L transport 2-amino-2-norbornanecarboxylic (BCH) at a final concentration of 10 mM or HBSS as a control. Kynurenine (KYN) was added to the cell suspension at a final concentration of 200 μM. For live cell uptakes data was acquired on a flow cytometer immediately following KYN addition. KYN uptake was also assessed for a fixed time of 4 min after which time cells were fixed with paraformaldehyde at a final concentration of 1% and analyzed by flow cytometry.

Rates of protein synthesis were measured using a click-chemistry reaction and flow cytometry. Cervical, axillary, brachial and inguinal lymph nodes were extracted from wildtype mice, and B cells were activated ± rapamycin for 24 h as described above. B cells were incubated for 20 min with O-propargyl-puromycin (OPP, Jena Bioscience), and the incorporation of the aminoacyl-tRNA mimetic into newly synthesized polypeptides was measured by labeling the OPP was with Alexa 647-azide (Invitrogen) using a copper-catalysed click-chemistry reaction (Invitrogen). Cells were analyzed using an LSR flow cytometer and analyzed with FlowJo software (Treestar).

Proteomics sample preparation and peptide fractionation

For all proteomics experiments except *Myc* knockout, cell pellets were lysed in 400 μL of lysis buffer (5% sodium dodecyl sulfate, 50 mM triethylammonium bicarbonate (pH 8.5) and 10 mM tris(2-carboxyethyl)phosphine-hydrochloride). Lysates were shaken at room temperature at 1000 rpm for 5 min and then incubated at 95 °C at 500 rpm for 5 min. Samples were allowed to cool before being sonicated using a BioRuptor (15 cycles: 30 s on and 30 s off) and alkylated with 20 mM iodoacetamide for 1 h at 22 °C in the dark. Protein concentration was determined using the EZQ protein quantitation kit (Invitrogen) and protein cleanup and digestion was performed using S-TRAP mini columns (Protifi). Proteins were digested with trypsin at 1:20 ratio (enzyme:protein) for 2 h at 47°C. Digested peptides were eluted from S-TRAP columns using 50 mM ammonium bicarbonate, followed by 0.2% aqueous formic acid and 50% aqueous acetonitrile containing 0.2% formic acid. Peptides were dried by speedvac before resuspending in 1% formic acid for fractionation.

For naive, activated and rapamycin B cell proteomes peptides were fractionated using high pH reverse-phase chromatography. Peptides were loaded onto a XbridgeTM BEH130 C18 column with 3.5 μm particles (Waters). Using a Dionex BioRS system, the samples were separated using a 25-min multistep gradient of solvents A (10 mM formate at pH 9 in 2% acetonitrile) and B (10 mM ammonium formate at pH 9 in 80% acetonitrile), at a flow rate of 0.3 mL/min. Peptides were separated into 16 fractions which were concatenated into 8. Fractions were dried and the peptides were dissolved in 1% formic acid and analyzed by liquid chromatography–mass spectrometry.

For *Myc* knockout proteomes, cell pellets were resuspended in 4% SDS in 100 mM Tris pH 7.6 with 10 mM DTT and lysed by sonication in a Bioruptor (Diagenode, 15 cycles, 30s on, 30s off, high mode), followed by a 10 min incubation at 95°C in agitation. The lysates were alkylated with 50 mM iodoacetamide for 30 min at room temperature, cleared by centrifugation for 5 min at maximum speed, and proteins were precipitated overnight in 80% cold acetone at −20°C. The next day, proteins were pelleted by centrifugation at 13,000 RPM for 20 min at 4°C, after which the pellets were dried and resuspended in 8M urea in 50 mM ammonium bicarbonate by Bioruptor sonication. For each sample, an initial digestion was performed on 100 μg of protein with LysC (Wako Fujifilm, 1:100 w/w) for 2 h at room temperature, after which the digestion buffer was diluted to 2M urea with 50 mM ammonium bicarbonate and trypsin (Promega, 1:100 w/w) was added for overnight digestion at room temperature. Digestion was stopped in 2% acetonitrile (ACN) and 0.3% trifluoroacetic acid (TFA) and the samples were cleared by centrifugation for 5 min at maximum speed. Peptides were purified on C18 StageTips,[89] and eluted with 80% ACN, 0.5% acetic acid. Finally, the elution buffer was removed by vacuum centrifugation and purified peptides were resolved in 2% ACN, 0.5% acetic acid, 0.1% TFA for single-shot LC-MS/MS measurements.

Liquid chromatography mass spectrometry analysis (LC- MS/MS)

For naive, activated and rapamycin B cell proteomes samples were analyzed by data dependent acquisition (DDA). 1.5 μg of peptide was injected onto a nanoscale C18 reverse-phase chromatography system (UltiMate 3000 RSLC nano, Thermo Scientific) and electrosprayed into an Q Exactive Plus mass spectrometer (Thermo Fisher). Buffers used for liquid chromatography were: buffer A (0.1% formic acid in Milli-Q water (v/v)) and buffer B (80% acetonitrile and 0.1% formic acid in Milli-Q water (v/v). Samples were loaded at 10 μL/min onto a trap column (100 μm × 2 cm, PepMap nanoViper C18 column, 5 μm, 100 Å, Thermo Scientific) equilibrated in 0.1% trifluoroacetic acid (TFA). The trap column was washed for 3 min at the same flow rate with 0.1% TFA then switched in-line with a Thermo Scientific, resolving C18 column (75 μm × 50 cm, PepMap RSLC C18 column, 2 μm, 100 Å). Peptides were eluted from the column at a constant flow rate of 300 nL/min with a linear gradient from 3% buffer B to 6% buffer B in 5 min, then from 6% buffer B to 35% buffer B in 115 min, and finally to 80% buffer B within 7 min. The column was washed with 80% buffer B for 4 min and re-equilibrated in 3% buffer B for 15 min. Two blanks were run between each sample to reduce carry-over. The column was kept at a constant temperature of 50°C.

The data was acquired using an easy spray source operated in positive mode with spray voltage at 2.445 kV, and the ion transfer tube temperature at 250°C. The MS was operated in DDA mode. A scan cycle comprised a full MS scan (m/z range from 350–1650), with RF lens at 40%, AGC target set to custom, normalised AGC target at 300, maximum injection time mode set to custom, maximum injection time at 20 ms and source fragmentation disabled. MS survey scan was followed by MS/MS DIA scan events using the following parameters: multiplex ions set to false, collision energy mode set to stepped, collision energy type set to normalized, HCD collision energies set to 25.5, 27 and 30, orbitrap resolution 30000, first mass 200, RF lens 40, AGC target set to custom, normalized AGC target 3000, maximum injection time 55 ms.

To generate proteomes examining the impact of MYC inhibition and the impact of individual and combined stimuli on B cells, peptides were analyzed by data independent acquisition (DIA).[90–92] 1.5 μg of peptides was injected onto a nanoscale C18 reverse-phase chromatography system (UltiMate 3000 RSLC nano, Thermo Scientific) and electrosprayed into an Orbitrap Exploris 480 Mass Spectrometer (Thermo Fisher). The following liquid chromatography buffers were used: buffer A (0.1% formic acid in Milli-Q water (v/v)) and buffer B (80% acetonitrile and 0.1% formic acid in Milli-Q water (v/v). Samples were loaded at 10 μL/min onto a trap column (100 μm × 2 cm, PepMap nanoViper C18 column, 5 μm, 100 Å, Thermo Scientific) equilibrated in 0.1% trifluoroacetic acid (TFA). The trap column was washed for 3 min at the same flow rate with 0.1% TFA then switched in-line with a Thermo Scientific, resolving C18 column (75 μm × 50 cm, PepMap RSLC C18 column, 2 μm, 100 Å). Peptides were eluted from the column at a constant flow rate of 300 nL/min with a linear gradient from 3% buffer B to 6% buffer B in 5 min, then from 6% buffer B to 35% buffer B in 115 min, and finally to 80% buffer B within 7 min. The column was then washed with 80% buffer B for 4 min and re-equilibrated in 3% buffer B for 15 min. Two blanks were run between each sample to reduce carry-over. The column was kept at a constant temperature of 50 °C.

The data was acquired using an easy spray source operated in positive mode with spray voltage at 2.445 kV, and the ion transfer tube temperature at 250 °C. The MS was operated in DIA mode. A scan cycle comprised a full MS scan (m/z range from 350 to 1650), with RF lens at 40%, AGC target set to custom, normalised AGC target at 300%, maximum injection time mode set to custom, maximum injection time at 20 ms, microscan set to 1 and source fragmentation disabled. MS survey scan was followed by MS/MS DIA scan events using the following parameters: multiplex ions set to false, collision energy mode set to stepped, collision energy type set to normalized, HCD collision energies set to 25.5, 27 and 30%, orbitrap resolution 30,000, first mass 200, RF lens 40%, AGC target set to custom, normalized AGC target 3000%, microscan set to 1 and maximum injection time 55 ms. Data for both MS scan and MS/MS DIA scan events were acquired in profile mode.

For *Myc* knockout proteomes, peptides were separated on a nanoElute2 HPLC system (Bruker) coupled via a nanoelectrospray source (Captive spray source, Bruker) to a timsTOF HT mass spectrometer (Bruker). 500 ng of peptides per sample were loaded in water with 0.1% formic acid into a column (25 cm long, 75 μm inner diameter, kept at 50°C in a column oven) in-house packed with ReproSil-Pur C18-AQ 1.9 μm resin (Dr. Maisch HPLC GmbH), and eluted over a 60-min linear 2–35% gradient of ACN with 0.1% formic acid at a 300 nL/min flow rate. The mass spectrometer was operated in a data-independent (DIA)-PASEF mode with 100 ms of accumulation and ramp time, covering with 21 mass steps, 25 Da wide, and 1 mobility window, a mass range from 475 to 1000 Da and a mobility range from 0.85 to 1.27 Vs. cm-2, with an estimated cycle time of 0.95 s.

Proteomics data processing and analysis

Data dependent mass spectrometry raw files were searched using MaxQuant[93] (version 1.6.10.43). Data was searched against a hybrid database from Uniprot release 06/2020. This hybrid database comprised of all manually annotated mouse SwissProt entries combined with mouse TrEMBL entries with protein level evidence available and a manually annotated homologue within the human SwissProt database. The false discovery rate was set to 1% for positive identification at the protein and peptide level. Protein N-terminal acetylation, methionine oxidation and deamidation (NQ) were set as variable modifications and carbamidomethylation of cysteine residues was selected as a fixed modification. Match between runs was disabled. Proteins categorized as 'contaminants', 'reverse' and 'only identified by site' were removed. Data independent mass spectrometry raw files were searched using Spectronaut (Biognosys) version 19. Raw mass spec files were searched against a mouse database (Swissprot Trembl November 2023) with the following parameters: directDIA, false discovery rate set to 1%, protein N-terminal acetylation and methionine oxidation were set as variable modifications and carbamidomethylation of cysteine residues was selected as a fixed modification. Copy numbers were calculated using the proteomic ruler[28] using Perseus software[94] except for *Myc* KO data which was normalised against the median

intensity for each sample. GO term enrichment analysis was performed using the ORA algorithm from the R Bioconductor package clusterProfiler. The annotation database was set to GO biological process (GOBP) and the organism database used was org.Mm.e.g.,.db. A secondary simplification step was performed to remove redundancies from GO enrichment results (default settings were used with a similarity cut-off of 0.6).

QUANTIFICATION AND STATISTICAL ANALYSIS

For proteomics data, protein differential expression analysis was performed using R (v. 4.0.3) and *p*-values and fold changes were calculated using the Bioconductor package Limma (v 3.46.0)[95] and a two-tailed empirical Bayes moderated *t* test. All other statistical testing was performed using GraphPad Prism software (v. 10) with details of statistical tests provided within figure legends.